Analysis of the low-energy $\pi^- p$ charge-exchange data

E. Matsinos* [a], G. Rasche [b],

[a] *Centre for Applied Mathematics and Physics, Zurich University of Applied Sciences, Technikumstrasse 9, P.O. Box, CH-8401 Winterthur, Switzerland*

[b] *Institut für Theoretische Physik der Universität, Winterthurerstrasse 190, CH-8057 Zürich, Switzerland*

*Corresponding author. E-mail: evangelos.matsinos@zhaw.ch, evangelos.matsinos@sunrise.ch; Tel.: +41 58 9347882; Fax: +41 58 9357306

Abstract

We analyse the charge-exchange (CX) measurements $\pi^- p \to \pi^0 n$ below pion laboratory kinetic energy of 100 MeV. After the removal of five degrees of freedom from the initial database, we combined it with the truncated $\pi^+ p$ database of Ref. [1] and fitted to the data using the ETH model [6]. The set of model-parameter values, as well as the predictions (which are derived on their basis) for the phase shifts and for the low-energy πN constants, are significantly different from the results we obtained in the analysis of the truncated $\pi^\pm p$ elastic-scattering databases. Concerning the phase shifts, the main difference occurs in $\tilde{\delta}^{1/2}_{0+}$; smaller differences have been found in two p-wave phase shifts. We discuss the implications of these findings in terms of the violation of the isospin invariance in the hadronic part of the πN interaction. The effect observed is at the level of $7 - 8\%$ in the CX scattering amplitude below about 70 MeV. The results and conclusions of this study agree very well with those obtained in the mid 1990s, when the isospin invariance was first tested by using πN experimental data, and disagree with the predictions obtained within the framework of the heavy-baryon Chiral-Perturbation Theory.

PACS: 13.75.Gx; 25.80.Dj; 25.80.Gn

Key words: πN hadronic phase shifts; πN coupling constants; πN threshold parameters; isospin-invariance violation; isospin breaking

1 Introduction

This is the last of three papers addressing issues of the pion-nucleon (πN) interaction at low energies (pion laboratory kinetic energy $T \leq 100$ MeV). In the first paper [1], we reported on a new phase-shift analysis (PSA) of the $\pi^{\pm}p$ elastic-scattering measurements. In the second paper [2], we examined the self-consistency of the large $\pi^{\pm}p$ elastic-scattering set of Ref. [3], which has not been included in our PSAs. In the present study, we will analyse the experimental data for the charge-exchange (CX) reaction $\pi^{-}p \to \pi^{0}n$ and investigate whether earlier claims on the isospin breaking [4,5] need, in view of the impressive increase of the CX database and of the development of our analysis methods during the last fifteen years, to be revised.

We will mark the physical quantities extracted in the analysis of the $\pi^{\pm}p$ elastic-scattering data [1] with the label 'ZUAS12'; this applies both to the solution obtained for the parameters of the ETH model [6] and for the hadronic phase shifts, as well as to the predictions derived on the basis of Tables 3 (for $\mathrm{p}_{min} \approx 1.24 \cdot 10^{-2}$) and 4 of Ref. [1]. The corresponding results, obtained in the present work from the common analysis of the $\pi^{+}p$ and CX databases, will be marked with the label 'ZUAS12a'.

Similarly to Ref. [1], we will assume that the physical quantities appearing in the present study (i.e., the fit parameters of Sections 4.1 and 4.2, the scattering lengths and volumes of Section 4.2.1, the phase shifts of Section 4.2.2, etc.) are not purely-hadronic quantities since they still contain residual electromagnetic (em) effects. As, however, the repetitive use of the term 'em-modified' is clumsy, we will omit it, unless we consider its use necessary as, for instance, in the captions of our tables and figures, as well as in Section 7.

2 Method

The formalism which we use here has been described in detail in Ref. [7]. The determination of the observables from the hadronic phase shifts may be found in Section 2 of that work. For $\pi^{+}p$ scattering, one obtains the partial-wave amplitudes from Eq. (1) and determines the no-spin-flip and spin-flip amplitudes via Eqs. (2) and (3). The observables are obtained from these amplitudes via Eqs. (13) and (14). For the CX reaction, the observables are determined using Eqs. (21-24) of Ref. [7].

All the details on the analysis method (i.e., on the minimisation function, on the scale factors, etc.) may be found in Section 2.2 of Ref. [1]. The contribution χ^2_j of the j^{th} data set to the overall χ^2 is given therein by Eq. (1). The scale

factors z_j, which minimise each χ^2_j, are evaluated using Eq. (2); the minimal χ^2_j value for each data set (denoted by $(\chi^2_j)_{min}$) is given in Eq. (3) and the scaling contribution (of the j^{th} data set) to $(\chi^2_j)_{min}$ in Eq. (4). Finally, the scale factors for free floating $\hat{z}_j$ (which we will use in Section 5, when investigating the absolute normalisation of the CX data using the ZUAS12 prediction as reference) are obtained from Eq. (5); their total uncertainty $\Delta\hat{z}_j$ has been defined at the end of Section 2.2 of Ref. [1].

One statistical test will be performed for each data set, the one involving its contribution $(\chi^2_j)_{min}$ to the overall χ^2. The corresponding p-value will be evaluated on the basis of $(\chi^2_j)_{min}$ and of the number of degrees of freedom of the data set (hereafter, the acronym DOF will stand for 'degree(s) of freedom', whereas NDF will denote the 'number of DOF'); for a data set with N_j data points (none of which is an outlier), NDF is equal to N_j. The p-value for each data set will be compared to the confidence level p_{min} for the acceptance of the null hypothesis (implying no statistically-significant effects). The value of p_{min} is fixed to the equivalent of a 2.5σ effect in the normal distribution, corresponding to about $1.24 \cdot 10^{-2}$.

The repetitive use of the full description of the databases is largely facilitated if we adhere to the following notation: DB_+ for the π^+p database; DB_- for the π^-p elastic-scattering database; DB_0 for the CX database; $DB_{+/-}$ for the combined $\pi^\pm p$ elastic-scattering databases; $DB_{+/0}$ for the combined π^+p and CX databases.

3 The CX data

The available CX measurements are listed (in the chronological order in which they had been reported) in Table 1. During the last fifteen years, the database has been increased sevenfold, i.e., from a mere 47 data points (which were available for the analyses [4,5]) to the present status of a total of 333 data points. Of the added 286 data points, 270 relate to the differential cross section (DCS), 9 to the total cross section (TCS), 6 to the analysing power (AP), and 1 data point to one threshold constant (to the isovector scattering length b_1).

A milestone in the low-energy CX experimentation was the FITZGERALD86 [11] experiment which took place at the Clinton P. Anderson Meson Physics Facility (LAMPF) and used the π^0 spectrometer to obtain (for the first time) important DCS data around the s- and p-wave interference minimum (see next section). By establishing a rigorous relation between the real parts of the s- and p-wave CX amplitudes at low energies, the FITZGERALD86 experiment became the backbone of the analyses [4,5] and was essential in terms of their conclusions on the violation of the isospin invariance in the hadronic part of

the πN interaction. The FITZGERALD86 experiment was the first complete CX experiment, as it also investigated (and reported) the normalisation uncertainty. Important in terms of the enhancement of the DB_0, shortly before the millenium change, was the ISENHOWER99 [16] experiment, also performed at LAMPF with the π^0 spectrometer.

Within the last decade, the Crystal-Ball Collaboration made massive contributions to the low-energy DB_0 by perfoming experiments at the Brookhaven National Laboratory (BNL): the SADLER04 [18] experiment added 60 data points, whereas the successor of that experiment, the MEKTEROVIĆ09 [21] experiment, contributed another 140 data points. In total, the data obtained by the Crystal-Ball Collaboration amount now to 60% of the entire DB_0 available below 100 MeV.

From the remaining experiments, the JIA08 [20] data have been taken around the s- and p-wave interference minimum, whereas the SCHROEDER01 [17] experimental result on the width of the $1s$ state in pionic hydrogen (corrected in Ref. [22] after properly taking into account the contributions of the γn channel) led to the extraction of the scattering length a^{c0} ($= \sqrt{2}b_1$). The FRLEŽ98 [14] experiment investigated the angular distribution of the DCS at 27.50 MeV. Finally, the BREITSCHOPF06 [19] experiment reported the CX TCSs at nine energies below 100 MeV. The remaining experiments account for less than 10% of the DB_0 at low energies.

The full DB_0 consists of 54 data sets. The quoted values of the TCS in Refs. [10,12,21] have been extracted from the coefficients of the Legendre expansion of the angular distribution of the DCS and are thus correlated with the main results of these experiments; because of this correlation, one may use either set of values, but not both. We will use the Legendre coefficients of Refs. [10,12] (their DCS measurements have not been published), and directly the DCS data of Ref. [21].

In our approach, all data sets must be accompanied by a normalisation uncertainty. This requirement also applies to one-point data sets, because the scale factors must be calculated in all cases (in order to enable the investigation of a possible bias in the analysis). As a result, we had to assign realistic normalisation uncertainties to those experiments which did not report this quantity. We decided to assign these uncertainties as follows:

- 6% to BUGG71 [8], as the experiments of the TCS or PTCS were assigned this uncertainty in Refs. [1,7].
- 3% to BREITSCHOPF06, because the experimental group had already combined statistical and systematic effects in quadrature (and reported only the total uncertainty).
- 3.1% to SALOMON84 [10], i.e., the normalisation uncertainty of the (very

similar, as well as close in time) BAGHERI88 [12] experiment.
- 8% to DUCLOS73 [9], i.e., double the normalisation uncertainty of the ISENHOWER99 large-angle data sets.

The experimental results of Ref. [20] contain asymmetric statistical uncertainties for the measured DCS. Unable to treat asymmetric uncertainties in our analysis, we will use the average of the two uncertainties for each input data point.

4 The s- and p-wave interference minimum

The main contributions to the CX scattering amplitude in the low-energy region come from the real parts of the s and p waves. These contributions are of opposite signs and they cancel each other in the forward direction around 45 MeV. This destructive-interference phenomenon acts as a magnifying glass, probing the smaller contributions in the πN dynamics, like those from the imaginary parts, from the d and f waves, and (potentially) from isospin breaking.

An estimation of the energy of the CX DCS minimum has been obtained in the FITZGERALD86 experiment, from an extrapolation of their DCS measurements to centre-of-mass (CM) scattering angle $\theta = 0°$. According to that estimation, the DCS minimum occurs at pion CM kinetic energy $\epsilon \sim 33$ MeV or $T \sim 45$ MeV; the minimal DCS value was also extracted: 2.4 ± 0.5 μb/sr [11]. The energy of the s- and p-wave interference minimum has been obtained on the basis of the ZUAS12 solution; the prediction is close to 43.7 MeV, whereas the minimal DCS falls well below 1 μb/sr. Both predictions (i.e., of the energy of the minimum and of the minimal DCS value) do not seem to match well the estimation of Ref. [11].

4.1 Fits to the DB_0 using the K-matrix expansions

As when analysing the DB_- in Section 3.2 of Ref. [1], we will fix the $I = 3/2$ amplitudes from the final fit to the truncated DB_+ using the K-matrix expansions (see Section 3.1 of that paper). The same K-matrix expansions for the $I = 1/2$ amplitudes will be used for the description of the CX measurements, of course, with different parameters $\tilde{a}^{1/2}_{0+}$, b_1, c_1, d_{13}, e_{13}, d_{11}, and e_{11}.

The χ^2 value of the first fit to the data was 400.3 for 326 DOF in the fit, indicating a rather coherent database. On the basis of the results of this fit, we had to freely float the FITZGERALD86 data set at 40.26 MeV. The second

run yielded a χ^2 value of 375.1; we had to freely float the FITZGERALD86 data set at 36.11 MeV. The third run yielded a χ^2 value of 351.5; we also had to freely float the FITZGERALD86 data set at 32.48 MeV. Interestingly, the removal of these three DOF from the initial DB_0 led to the decrease of the χ^2 by 66.9 units.

Two additional runs were sufficient in removing all outliers from the DB_0. In the first run, the one-point data set of the BREITSCHOPF06 experiment at 75.10 MeV had to be removed, whereas the absolute normalisation of another FITZGARALD86 data set (at 47.93 MeV) was removed in the second. The final fit to the data yielded the χ^2 value of 312.8 for 321 DOF in the fit. The optimal values of the parameters $\tilde{a}_{0+}^{1/2}$, d_{13}, and e_{13} came out significantly different [1] from the ones obtained in the analysis of the DB_- in Ref. [1].

Although the results obtained so far provide a firm basis for questioning the absolute normalisation in all seven FITZGERALD86 data sets, we will retain the absolute normalisation of the three remaining FITZGERALD86 data sets as their removal is not called for when strictly following our rejection criteria. On the other hand, given the importance of FITZGERALD86 data in Refs. [4,5], it is obvious that the re-analysis of the CX measurements in terms of the violation of the isospin invariance in the hadronic part of the πN interaction at low energies is imperative.

4.2 Common fit to the truncated $DB_{+/0}$ using the ETH model

Details on the ETH model, as well as on its seven parameters (G_σ, K_σ, G_ρ, K_ρ, $g_{\pi NN}$, $g_{\pi N\Delta}$, and Z) may be obtained from Refs. [7,1]. This isospin-invariant model was introduced in Ref. [6] and was developed to its final form by the mid 1990s.

Prior to fitting the ETH model to the truncated $\mathrm{DB}_{+/0}$, we subjected the data to a common fit using the K-matrix expansions. At that moment, the truncated DB_+ consisted of 340 data points (detailed in Table 1 of Ref. [1]), whereas the truncated DB_0 comprised 328 data points, i.e., the original 333 data points minus the five outliers detailed in the previous section. The common fit to these data using our K-matrix expansions resulted in the χ^2 value of 737.0 for 654 DOF in the fit and no outliers.

The model fit to the data yielded the minimal χ^2 value of 932.3 for 661 DOF. The optimal values for the model parameters from the fits to the truncated $\mathrm{DB}_{+/0}$ are given in Table 3; the uncertainties contain the Birge factor

[1] The differences between the two sets of values represent effects between 4.9 and 7.4σ in the normal distribution.

$\sqrt{\chi^2/\mathrm{NDF}}$, which takes account of the goodness of the fit. The table also contains the ZUAS12 solution for $\mathrm{p}_{min} \approx 1.24 \cdot 10^{-2}$. The differences between these two sets of model-parameter values are significant.

It is now time to reflect on the important χ^2 values obtained so far in our program. We first concentrate in the results for $\mathrm{p}_{min} \approx 1.24 \cdot 10^{-2}$. The separate fits to the data using the K-matrix expansions yielded the χ^2 values of 427.2, 371.0 [1], and 312.8 (this work) for the truncated DB_+, DB_-, and DB_0, with 333, 321, and 321 DOF in the fit, respectively. The χ^2 values obtained with the K-matrix expansions in the two analyses of the combined truncated databases (i.e., $\mathrm{DB}_{+/-}$ and $\mathrm{DB}_{+/0}$) come out very close to the sum of the corresponding results for the separate fits: 792.4 (instead of the sum of 798.1) for the truncated $\mathrm{DB}_{+/-}$ [1], 737.0 (instead of the sum of 740.0) for the truncated $\mathrm{DB}_{+/0}$ (this work). (As the NDF in the truncated DB_- and DB_0 are (by chance) identical, the results are directly comparable.) Therefore, we observe that, in the case of the fits using the K-matrix expansions, the difference of the two χ^2 values (which is about 55.4 units) reflects, almost entirely, the difference of the χ^2 values in the separate fits to the truncated DB_- and DB_0 using the K-matrix expansions (which is equal to 58.1 units, the smaller χ^2 value corresponding to the fit to the truncated DB_0).

The increase of the χ^2 values in the fits to the truncated $\mathrm{DB}_{+/-}$ using the ETH model (over the result of the fits to the same data using the K-matrix expansions) is due to the imposition of theoretical constraints (e.g., of the crossing and isospin symmetry); as earlier mentioned, the fits to the data using the K-matrix expansions are devoid of theoretical constraints, other than the expected low-energy behaviour of the K-matrix elements. All else being equal, one would expect that the difference in the χ^2 values between the model fit to the data and the fit using the K-matrix expansions would be (more or less) the same for the two truncated databases, i.e., for the $\mathrm{DB}_{+/-}$ and $\mathrm{DB}_{+/0}$, inasmuch as the same parameterisation is used in the modelling of the two $I = 1/2$ amplitudes; however, this is far from true. In the case of the common fit to the $\mathrm{DB}_{+/0}$, the difference between the two χ^2 values (i.e., for the model fit versus the one using K-matrix expansions) is so large that, though the separate fits to the truncated DB_0 using the K-matrix expansions yield χ^2 values significantly smaller than those for the truncated DB_-, the χ^2 value for the model fit to the truncated $\mathrm{DB}_{+/0}$ exceeds by far the one obtained from the truncated $\mathrm{DB}_{+/-}$. Evidently, the substitution of the truncated DB_- with DB_0 leads to a noticeable deterioration of the overall description of the experimental data in the model fits. This deterioration is indicative of a general difficulty in the description of the truncated $\mathrm{DB}_{+/0}$ in terms of *one* set of model-parameter values. This fact can be explained if the theoretical basis upon which the data analysis rests (presumably, the isospin invariance in the hadronic part of the πN interaction) is somewhat disturbed. Inspection of Table 5 shows that the information which is obtained from the data for the two other p_{min} levels

used in Ref. [1] (i.e., those corresponding to a 2 and 3σ effect in the normal distribution) is very consistent with the result for $p_{min} \approx 1.24 \cdot 10^{-2}$. We will return to this issue in Section 6.3.

4.2.1 Threshold constants

From the model parameters and their uncertainties given in Table 3, as well as the correlation matrix given in Table 4, we calculated the isoscalar and isovector s-wave scattering lengths and the isoscalar(isovector)-scalar(vector) p-wave scattering volumes. The results are:

$$\begin{aligned}
&\frac{1}{3}\,\tilde{a}_{0+}^{1/2} + \frac{2}{3}\,\tilde{a}_{0+}^{3/2} = 0.0060(24)\,\mu_c^{-1},\\
&-\frac{1}{3}\,\tilde{a}_{0+}^{1/2} + \frac{1}{3}\,\tilde{a}_{0+}^{3/2} = -0.08272(56)\,\mu_c^{-1},\\
&\frac{1}{3}\,\tilde{a}_{1-}^{1/2} + \frac{2}{3}\,\tilde{a}_{1-}^{3/2} + \frac{2}{3}\,\tilde{a}_{1+}^{1/2} + \frac{4}{3}\,\tilde{a}_{1+}^{3/2} = 0.2085(28)\,\mu_c^{-3},\\
&-\frac{1}{3}\,\tilde{a}_{1-}^{1/2} + \frac{1}{3}\,\tilde{a}_{1-}^{3/2} - \frac{2}{3}\,\tilde{a}_{1+}^{1/2} + \frac{2}{3}\,\tilde{a}_{1+}^{3/2} = 0.1834(17)\,\mu_c^{-3},\\
&\frac{1}{3}\,\tilde{a}_{1-}^{1/2} + \frac{2}{3}\,\tilde{a}_{1-}^{3/2} - \frac{1}{3}\,\tilde{a}_{1+}^{1/2} - \frac{2}{3}\,\tilde{a}_{1+}^{3/2} = -0.1943(17)\,\mu_c^{-3},\\
&-\frac{1}{3}\,\tilde{a}_{1-}^{1/2} + \frac{1}{3}\,\tilde{a}_{1-}^{3/2} + \frac{1}{3}\,\tilde{a}_{1+}^{1/2} - \frac{1}{3}\,\tilde{a}_{1+}^{3/2} = -0.0680(11)\,\mu_c^{-3}.
\end{aligned} \tag{1}$$

Converting these results to the familiar spin-isospin quantities, we obtain

$$\begin{aligned}
&\tilde{a}_{0+}^{3/2} = -0.0767(24)\,\mu_c^{-1}, \qquad \tilde{a}_{0+}^{1/2} = 0.1715(28)\,\mu_c^{-1},\\
&\tilde{a}_{1+}^{3/2} = 0.2181(19)\,\mu_c^{-3}, \qquad \tilde{a}_{1+}^{1/2} = -0.0334(10)\,\mu_c^{-3},\\
&\tilde{a}_{1-}^{3/2} = -0.0443(12)\,\mu_c^{-3}, \qquad \tilde{a}_{1-}^{1/2} = -0.0916(23)\,\mu_c^{-3}.
\end{aligned} \tag{2}$$

Significant differences are found when comparing the values of $\tilde{a}_{0+}^{1/2}$, $\tilde{a}_{1+}^{3/2}$, and $\tilde{a}_{1-}^{1/2}$ with the corresponding results of Ref. [1].

From the results in Eqs. (2), we obtain

$$\tilde{a}^{cc} = \frac{2}{3}\,\tilde{a}_{0+}^{1/2} + \frac{1}{3}\,\tilde{a}_{0+}^{3/2} = 0.0888(26)\,\mu_c^{-1}$$

and

$$\tilde{a}^{c0} = \sqrt{2}\left(-\frac{1}{3}\,\tilde{a}_{0+}^{1/2} + \frac{1}{3}\,\tilde{a}_{0+}^{3/2}\right) = -0.11698(79)\,\mu_c^{-1}\,.$$

Unlike the $\tilde{a}^{cc}$ value extracted from the truncated $\mathrm{DB}_{+/-}$ [1], the value of the present work is compatible with the result of the measurement of the strong shift of the $1s$ state in pionic hydrogen [17]. Additionally, the value of $\tilde{a}^{c0}$ is marginally consistent (the difference between the two values is at the level of 1.8σ) with the result of the same experiment for the width of the $1s$ state in pionic hydrogen. (In this comparison, we have corrected the raw experimental results of Ref. [17] with the em corrections of Ref. [22].)

4.2.2 Hadronic phase shifts

The s- and p-wave hadronic phase shifts, from the fit to the truncated $\mathrm{DB}_{+/0}$ using the ETH model, are given in Table 6. These hadronic phase shifts are also shown in Figs. 1-6, together with the ZUAS12 results, as well as the current SAID solution (WI08) [23] and their five single-energy values (whenever available). A very noticeable difference between the phase-shift results of the present work and those obtained in Ref. [1] may be seen in the case of the $\tilde{\delta}_{0+}^{1/2}$ phase shift. Smaller differences may be seen in two p-wave phase shifts, in $\tilde{\delta}_{1+}^{3/2}$ and $\tilde{\delta}_{1-}^{1/2}$.

4.2.3 Scale factors and normalised residuals

We will next provide evidence that the outcome of the common fit of the present work is reliable. Similarly to the tests performed in Section 3.4.4 of Ref. [1], we will first investigate whether any bias may be seen in the distribution of the scale factors z_j, extracted in the final step of the optimisation scheme. Subsequently, we will address the issue of the distribution of the normalised residuals of the fit.

For both the π^+p (Fig. 7) and CX (Fig. 8) data sets, the values of z_j which lie above and below 1 roughly balance each other and there is no discernible energy dependence; a small effect may be present at very low energies (i.e., in the scale factors of five of the ISENHOWER99 experiments), yet it does not seem to be significant. All taken into account, there is no subrange of the entire energy interval in which the data is better or worse fitted than for the rest of the range.

The distribution of the normalised residuals is shown in Fig. 9, along with the optimal Gaussian function. The χ^2 value of this fit was 23.6 for 22 DOF,

whereas the offset $\bar{r}$ (for the definition, see Section 3.4.4 of Ref. [1]) comes out equal to $(-9.3 \pm 4.0) \cdot 10^{-2}$. A shift in the distribution, indicating a slight underestimation of the 'theoretical' values y_{ij}^{th} in the fit, is visible in Fig. 9. However, as the result for $\bar{r}$ indicates, one may obtain an acceptable description of the data by fixing $\bar{r}$ to 0. For the sake of completeness, we also give the optimal value and the uncertainty of parameter B of the Gaussian fit to the data: $B = 0.501 \pm 0.035$; the expectation value for B is 0.5.

5 Investigation of the absolute normalisation of the CX data on the basis of the ZUAS12 solution

We will next investigate the absolute normalisation of the CX data sets using the ZUAS12 solution as reference. To this end, we must determine the amount at which the predictions obtained on the basis of the reference solution for each CX data set (i.e., the y_{ij}^{th} values appearing in Eq. (1) of Ref. [1]) must be floated in order to optimally fit the data set in question. Therefore, relevant in this part of the analysis are the scale factors for free floating $\hat{z}_j$, given in Eq. (5) of Ref. [1].

The extracted values of the scale factors $\hat{z}_j$ and their total uncertainties may be found in Table 7 and, plotted separately for the DCS, TCS, AP, and LEC data sets, in Fig. 10. The four FITZGERALD86 data sets which had been freely floated in Section 4.1 are not shown; their $\hat{z}_j$ factors came out equal to 2.03(14), 2.26(15), 2.28(14), and 1.52(13) (the order corresponds to increasing energy); evidently, something must have gone wrong in the determination of the absolute normalisation of these data sets. Even when using only the CX data, the scale factors obtained for these data sets (see Table 2) are significantly larger than the expectation value of 1. The $\hat{z}_j$ factor of the one-point data set of the BREITSCHOPF06 experiment which was eliminated in Section 4.1 came out equal to 0.927(50), indicating that this measurement is an outlier only when compared with the bulk of the CX data; this data point is also not shown in Fig. 10. One additional data point, the scattering length b_1 of Ref. [17], is not shown in this figure. In principle, one could assign this data point to the DCS set (after squaring the result for b_1), in which case the outcome would have been consistent with the scale factors for free floating of the ISENHOWER99 10.60 MeV data; however, we show only genuine DCS measurements in Fig. 10.

The careful inspection of Fig. 10 leaves no doubt that, when using the ZUAS12 solution as baseline, the CX scale factors for free floating contain a large amount of fluctuation. Given that the ZUAS12 solution is smooth, the fluctuation observed in Fig. 10 reflects the scattering of the absolute normalisation of the CX data. For instance, the $\hat{z}_j$ value for the FRLEŽ98 data set is equal

to 1.431(99). This data set lies in between three data sets with significantly smaller $\hat{z}_j$ values, i.e., between the two ISENHOWER99 20.60 MeV data sets and the MEKTEROVIĆ09 33.89 MeV data set. The two neighbouring data sets of DUCLOS73 (22.60 and 32.90 MeV), as well as the JIA08 34.37 MeV data set have $\hat{z}_j$ values compatible with 1.

Restricting ourselves below 70 MeV, we calculated the weighted average of the $\hat{z}_j$ factors of Table 7 and Fig. 10. Our result is that the low-energy CX measurements lie on average $(15.6 \pm 1.4)\%$ above the ZUAS12 predictions. Naively translated into a difference in the CX scattering amplitude, this result would be equivalent to an effect around the $7 - 8\%$ level.

In order to provide some perspective and, perhaps, motivation to research groups which are active in the low-energy πN experimentation, we will now give the predictions obtained on the basis of the ZUAS12 and ZUAS12a solutions in a number of situations. We will investigate the differences in these two prediction sets and identify the energy regions which provide fertile ground for distinguishing experimentally between the two sets of values. We commence with the DCSs and TCSs. (The results on the Legendre-expansion coefficients are expected to follow the sensitivity of the DCS.)

The two solutions around the s- and p-wave interference minimum are shown in Fig. 11 for $\theta = 0^\circ$. We observe that the energy corresponding to the DCS minimum comes out different in the two solutions; the ZUAS12a prediction exceeds the one obtained on the basis of the ZUAS12 results by about 1.2 MeV. Additionally, the ZUAS12a solution predicts a deeper DCS minimum.

The shapes of the angular distributions of the CX DCS, obtained on the basis of the ZUAS12 and ZUAS12a solutions, are different below and above the s- and p-wave interference minimum. Below the minimum, the ZUAS12a-based DCS systematically exceeds the one obtained from ZUAS12, by varying amounts; at 20 MeV, the relative difference (i.e., the difference normalised to the corresponding ZUAS12 values) is 17.7% for $\theta = 0^\circ$ decreasing to 12.2% at $\theta = 180^\circ$; the corresponding numbers for 30 MeV are: 24.0 and 11.4%; finally, at 40 MeV, the relative differences are: 59.1 and 10.4%. Evidently, the relative difference between the two predictions in the forward direction increases as the beam energy approaches the energy of the s- and p-wave interference minimum. Large effects are also seen in the TCS, slightly decreasing with increasing energy, from about 12.9% at 20 MeV, to 11.9% at 30 MeV, and to 10.7% at 40 MeV. A representative plot of the two predictions is given in Fig. 12 for 30 MeV.

The picture is slightly different at the higher end of the energies. The ZUAS12a result lies here below the ZUAS12 prediction in the forward direction. The two predictions cross each other between 40 and 90°; above the crossing, the

ZUAS12a prediction exceeds the ZUAS12 one (by smaller amounts when compared to the low energies). At 60 MeV, the relative difference between the two predictions at $\theta = 0^\circ$ is -11.6%, increasing to 8.4% at $\theta = 180^\circ$; at 80 MeV, the values are: -6.0 and 6.4%, whereas at 100 MeV, they are: -5.8 and 4.6%. At the same time, the net effect in the TCS decreases with increasing energy, from about 7.9% at 60 MeV, to 5.1% at 80 MeV, and to 2.5% at 100 MeV. A representative plot of the angular distribution of the CX DCS above the s- and p-wave interference minimum is shown in Fig. 13 for 80 MeV.

It is evident from our investigation that the AP shows high sensitivity to the effect under investigation around the s- and p-wave interference minimum. The few available measurements of the AP in the low-energy CX reaction have been taken at 98.10 and 100.00 MeV, where the differences between the two prediction sets are very small.

We will now comment on the recent experiment of Ref. [20], which took data at forward angles, at six energies around the s- and p-wave interference minimum. The authors make the point that their data 'show no evidence for unexpected isospin-breaking effects'. To start with, according to Table 2 and assuming the correctness of the normalisation of the bulk of the CX data, the JIA08 measurements lie between 0.5 and 1.5σ (σ, in this case, is equivalent to 10%) below the optimal solution obtained only from the CX data in Section 4.1. We created the ZUAS12 and ZUAS12a predictions corresponding to the values of the kinematical variables of these data. As seen in Figs. 14, these two solutions lie close to one another in the kinematical region of the measurements. As a result, the experiment indeed agrees with the ZUAS12 solution, but it also does with the ZUAS12a prediction (which was not available at the time the experimental paper appeared). Given the large normalisation uncertainties of the low-energy πN experiments, as well as the general closeness of the ZUAS12 and ZUAS12a solutions, it is rather unlikely that any single experiment will be capable of disproving the violation of the isospin invariance in the hadronic part of the πN interaction, especially one with a normalisation uncertainty at the 10% level.

We would like to stress that our predictions for the usual observables (DCS, TCS, AP), calculated on the basis of the ZUAS12 and ZUAS12a solutions, are available to all researchers in the πN field upon request; it takes very little effort to produce reliable results from our software on a grid of (θ,T) points. We must, however, draw attention to the correct interpretation of our numbers and figures both of the present work, as well as of any future communication (to πN research groups) as a response to a specific request. An agreement of the results of a CX experiment with the ZUAS12a solution may not be interpretted as unmistakable evidence for the violation of the isospin invariance in the hadronic part of the πN interaction (though such an agreement is in the right direction); it simply shows compatibility of the

experiment in question with the bulk of the CX data as analysed here. On the other hand, a significant disagreement of a CX experiment with the ZUAS12a solution points in the direction of potential problems with the integrity of the CX data; if, in this last case, the experimental results agree with the ZUAS12 prediction, then the interpretation can only be that the experiment does not support the possibility of the violation of the isospin invariance in the hadronic part of the πN interaction as it emerges in the present study.

6 Possible causes of the observed differences between the ZUAS12 and ZUAS12a solutions

We now summarise the main results obtained so far.

- Three of the values of the parameters of the K-matrix expansions (i.e., $\tilde{a}_{0+}^{1/2}$, d_{13}, and e_{13}), extracted in the analysis of the truncated $\mathrm{DB}_{+/0}$, differ significantly from those obtained in the analysis of the truncated $\mathrm{DB}_{+/-}$.
- Two of the values of the parameters of the ETH model (i.e., G_ρ and $g_{\pi NN}$), extracted in the analysis of the truncated $\mathrm{DB}_{+/0}$, differ significantly from those obtained in the analysis of the truncated $\mathrm{DB}_{+/-}$.
- When using the ETH model in the common fits to the data, the substitution of the truncated DB_{-} with DB_0 leads to obvious deterioration of the results, indicating difficulties in the description of these measurements in terms of *one* set of model-parameter values. In this respect, the results of Table 5, for the three values of p_{min} which have been used in Ref. [1], are very consistent.
- A significant difference has been seen in the s-wave phase shift $\tilde{\delta}_{0+}^{1/2}$; milder differences are observed in two p-wave phase shifts, i.e., in the $\tilde{\delta}_{1-}^{1/2}$ and in the $\tilde{\delta}_{1+}^{3/2}$.
- The reproduction of the absolute normalisation of the CX data sets on the basis of the ZUAS12 solution is very poor below about 70 MeV. The differences amount to a $7-8\%$ effect in the CX scattering amplitude.

These differences between the ZUAS12 and ZUAS12a solutions and the predictions obtained on their basis are significant. We will now attempt to identify possible causes of the observed discrepancies.

In view of these results, there are three hypotheses which cannot all be simultaneously valid.

- The bulk of the low-energy πN experimental data is reliable.
- The missing parts in the em corrections, applied to the experimental data in order to extract the hadronic part of the πN amplitude, are negligible.
- The isospin invariance in the hadronic part of the πN interaction is obeyed.

We will now elaborate on these three possibilities.

6.1 Experimental problems

The first explanation for the observed differences involves a trivial effect, i.e., the systematic incorrectness (overestimation or underestimation) of the absolute normalisation in the low-energy πN data. Furthermore, arguments have been presented in Ref. [7], to support the claim that the reported experimental uncertainties are underestimated. In this respect, the two elastic-scattering reactions seem to be more affected (than the CX).

Our first point concerns the statistical uncertainties of the data points. When visually inspecting the low-energy πN data, one is frequently unable to comprehend how it is possible for successive measurements (i.e., at neighbouring values of the CM scattering angle) to be so different. There are many occasions in the databases when one starts questioning the statistical uncertainties of the data points, which, in fact, should be the easiest to obtain in an experiment.

Our second point concerns the systematic effects. It is not understood how the absolute normalisation of some experiments, e.g., of the FITZGERALD86 data sets at the three lowest energies, may be wrong (according to the bulk of the truncated DB_0) by an average of about 70% (and of a fourth one by 45%), at a time when the reported normalisation uncertainty in the experiment was 7.8%. Such an effect may only be caused because of any of three reasons (or their combination): a) the determination of the absolute normalisation in the experiment has been erroneous, b) the energy of the incoming beam has not been what the experimenters expected, or c) the normalisation uncertainty in the experiment has been grossly underestimated.

Our third point concerns the small values of the normalisation uncertainty reported in many low-energy πN experiments; for instance, the reported normalisation uncertainty in 37 out of the 90 data sets in the initial $\mathrm{DB}_{+/-}$ is below 3%. One could possibly try to manipulate the normalisation uncertainty reported in such experiments (perhaps, by setting these values to 3%), yet such an approach would be arbitrary. Therefore, one must reluctantly accept the reported values. As a result, one must rely on an approach which places importance on the bulk of the experimental data and apply a reasonable procedure for the elimination of the outliers; this is the approach which we set up in Refs. [1,2,7].

There is one disturbing discrepancy in the entire analysis of the truncated $\mathrm{DB}_{+/-}$ which cannot be easily put aside, i.e., the disagreement between the $\tilde{a}^{cc}$ value obtained as an extrapolation from the experimental data (above the πN threshold) and the one extracted directly at the πN threshold from

the strong shift of the $1s$ level in pionic hydrogen. Assuming the correctness of both the bulk of the truncated DB$_-$ and of the raw measurement of ϵ_{1s} [17], the two extracted values should be compatible, if a consistent set of em corrections (i.e., corrections which have been obtained within the same framework), which is also complete in the sense of containing the contributions from all relevant physical effects, have been applied to the raw data. In case of any missing pieces in the em corrections (see next section), the question surfaces as to the energy dependence of the missing contributions. At present, there are no known effects which could invalidate the result from the pionic-hydrogen experiment [17] and, presumably, it is equally difficult to accept that the bulk of the truncated DB$_-$ is not reliable, especially as this set comprises measurements which 'cluster' together better than the ones for π^+p elastic scattering.

On the other hand, though there might be problems with the bulk of the low-energy πN experimental data, it is not at all clear how they can create the results of Table 5.

6.2 Missing pieces in the em corrections

Although it is not clear how these contributions can modify so drastically the overall picture and especially the results of Table 5 (any missing em contributions should be common in the description of the experimental data on the basis of the K-matrix expansions and of the ETH model), this is an important issue which must be properly defined and addressed. In Refs. [7,22], some details are given on the effects which the stage-II em corrections may contain. These effects are mostly related to the use of the (unknown) hadronic masses for the proton, the neutron, and the charged and neutral pion in the determination of the em corrections; the physical masses have been used in Refs. [28], which we apply in our program. Lacking, however, a consistent method for obtaining even a rough estimation of these contributions makes this discussion rhetorical and speculative. Until these values become available, there is no other option but to assume their smallness.

6.3 The violation of the isospin invariance in the hadronic part of the πN interaction

This is the third of the available options and, admittedly, the most exciting one in Physics terms. Interestingly, this possibility may easily provide an explanation for the results of Table 5. There has been a great amount of discussion regarding the acceptance of the conclusions of Refs. [4,5]. One, however, is tempted to pose the question: 'Why should the isospin invariance in the πN

system be obeyed in the first place?' After all, the hadronic masses of the u and d quarks are different; similarly, the masses of the nucleons differ (beyond trivial em effects), and so do those of Δ's. It appears, therefore, that the proper question is not whether the isospin invariance is violated, but at which amount it is. Within the framework of the heavy-baryon Chiral-Perturbation Theory, the group of Meißner has repeatedly treated isospin-breaking effects in the πN system at low energies and invariably concluded that such effects should be small, at the percent level at most (e.g., see Ref. [24] and the references cited therein).

Two mechanisms had been proposed in the past, to account for the violation of the isospin invariance in the hadronic part of the πN interaction at the level of Feynman diagrams: the first mechanism affects the elastic scattering ($\rho^0-\omega$ mixing [25]), the second the CX reaction ($\eta-\pi^0$ mixing [26]). As both the ω and the η states are singlets, the coupling of the former with the ρ^0 and of the latter with the π^0 explicitly violate the isospin invariance. Given that, in the case of the elastic scattering, only one graph (i.e., the t-channel ρ-exchange graph) is affected, whereas in the case of the CX reaction all Feynman diagrams are affected (see Fig. 15), one would be tempted to jump to the conclusion that the isospin-breaking effects are expected to be more important in the latter case; however, Ref. [26] concluded with the statement that '... the isospin violation from $\eta - \pi^0$ mixing can be safely ignored in πN partial-wave analyses.'

We noticed that the coupling constant $g_{\pi NN}$ is significantly affected when substituting the truncated DB$_-$ with DB$_0$. Of course, if the isospin invariance is violated, there is not *one* coupling constant $g_{\pi NN}$; one must distinguish between $g_{\pi^0 pp}$, $g_{\pi^0 nn}$, and $g_{\pi^\pm pn}$. In this case, the fits to the elastic-scattering data essentially determine $g_{\pi^\pm pn}$, whereas those involving the CX reaction will also contain contributions from $g_{\pi^0 pp}$ and $g_{\pi^0 nn}$. As a result, the value of the coupling constant $g_{\pi NN}$ extracted from the common fits to the truncated DB$_{+/0}$ represents a weighted average of these three quantities. The differences observed imply that at least one of the two $g_{\pi^0 NN}$ coupling constants is different from $g_{\pi^\pm pn}$. The isospin-breaking effects on these coupling constants have been studied theoretically and generally found small; for instance, Ref. [27] evaluated these effects with QCD sum rules and reported that $g_{\pi^\pm pn}$ should be equal to the average of the two $g_{\pi^0 NN}$ values, and that the splitting should be expected between 1.2 and 3.7%. The difference between the two $g_{\pi NN}$ values of Table 3 is larger, around the 4.5% level.

7 Discussion

The present study concludes our program of re-analysing the pion-nucleon (πN) data below pion laboratory kinetic energy of 100 MeV. The separate

analysis of the data for the two elastic-scattering and for the charge-exchange (CX) reactions was enabled via suitable expansions of the s- and p-wave K-matrix elements at low energies. Common fits to the data were performed using either these K-matrix expansions or the ETH model of Ref. [6], which is based on meson t-channel exchanges, as well as on the s- and u-channel N and Δ contributions. As a principle, the analysis with the K-matrix expansions was used in order to identify the obvious outliers in the databases and to test the self-consistency of the input prior to its submission to the fits using the ETH model. Given the freedom rendered to the input data in the analysis with the K-matrix expansions, any outliers in the fits can only be attributed to experimental problems. After the removal of the outliers, the databases were submitted to common fits using the ETH model. The optimal values of the model parameters, as well as their correlation matrix, are obtained from these fits and can be used as the basis for generating Monte-Carlo predictions for the phase shifts, for the low-energy πN constants, as well as for the standard observables (i.e., for the differential cross section (DCS), analysing power (AP), partial-total cross section (PTCS), and total cross section (TCS)) for any of the three reactions, at any value of the relevant kinematical variables (i.e., energy and scattering angle for the DCS and AP, energy and angle limit for the PTCS, and energy for the TCS).

Given that the electromagnetic (em) corrections (which are applied to the hadronic phase shifts in order to extract the πN partial-wave amplitudes, which, in turn, lead to the observables) of Ref. [28] have been obtained by using the physical, instead of the (unknown) hadronic, masses for the proton, the neutron, and the charged and neutral pion, we have assumed the cautious attitude of considering our physical quantities (i.e., the model parameters, the low-energy πN constants, the phase shifts, etc.) not purely hadronic, but em-modified hadronic. At the present time, one cannot give an estimation of the importance of the missing em effects (i.e., of the stage-II em corrections).

Following the procedure described in the first paragraph of the present section, we first analysed the two elastic-scattering reactions and obtained the solution (for the model parameters, as well as for the em-modified phase shifts) [1]. In this paper, we analysed the $\pi^+ p$ and CX databases. By comparing the results of these two PSAs, we found large effects both in the model parameters, as well as in the em-modified hadronic phase shifts. We have provided evidence that the differences are predominantly attributable to the s waves, in particular, to the em-modified phase shift $\tilde{\delta}^{1/2}_{0+}$; smaller differences have been found in two p-wave em-modified phase shifts.

Assuming the integrity of the bulk of the low-energy πN databases, as well as the smallness of the missing pieces in the em corrections (i.e., of the stage-II effects), these discrepancies can only be blamed on the violation of the isospin invariance in the hadronic part of the πN interaction at low energies. The

effect observed is at the level of $7-8\%$ in the CX scattering amplitude below about 70 MeV.

The results of this study agree very well with those obtained in the mid 1990s, when the isospin invariance in the πN system was first tested by using the available experimental information. This agreement is remarkable given the changes of the databases in the meantime (e.g., the CX database has been increased sevenfold), the analysis methods, and the em corrections which are applied to the experimental input data. Our results are in severe disagreement with predictions (for the isospin-breaking effect in the CX scattering amplitude), obtained within the framework of the heavy-baryon Chiral-Perturbation Theory; according to these estimations, the expected effects should be around the percent level.

In any analysis of experimental data, a question surfaces sooner or later: to what extent can the bulk of the data be trusted? The answer to this question in the case of the low-energy πN interaction is not simple. For a few years, we believed that, by excluding a small number of obvious outliers, we could obtain self-consistent databases. However, the analysis of the recently-obtained Denz et al.[3] measurements, which comprise a database of their own, led to numerous problems [2] mainly relating to the shape of the angular distributions of their $\pi^+ p$ differential cross sections. From the experimental point of view, it is as if we have not really advanced much after three decades of experimentation.

Acknowledgements

We acknowledge helpful discussions with W.R. Gibbs. We are grateful to T.P. Gorringe for communicating to us the measurements of Ref. [20]. We would like to thank W.S. Woolcock for his comments and suggestions.

References

[1] E. Matsinos, G. Rasche, 'Analysis of the low-energy $\pi^{\pm} p$ elastic-scattering data', submitted to Nuclear Physics A; available in http://arxiv.org.

[2] E. Matsinos, G. Rasche, 'Analysis of the DENZ04 low-energy $\pi^{\pm} p$ elastic-scattering data', submitted to Nuclear Physics A; available in http://arxiv.org.

[3] H. Denz et al., Phys. Lett. B 633 (2006) 209-13; the values of the elastic-scattering cross section are available from the site: http://tobias-lib.uni-tuebingen.de/dbt/volltexte/2004/1323/.

[4] W.R. Gibbs, Li Ai, W.B. Kaufmann, Phys. Rev. Lett. 74 (1995) 3740-3.

[5] E. Matsinos, Phys. Rev. C 56 (1997) 3014-25.

[6] P.F.A. Goudsmit, H.J. Leisi, E. Matsinos, B.L. Birbrair, A.B. Gridnev, Nucl. Phys. A 575 (1994) 673-706; more references on the development of the ETH model may be found at http://people.web.psi.ch/matsinos/0_home.htm.

[7] E. Matsinos, W.S. Woolcock, G.C. Oades, G. Rasche, A. Gashi, Nucl. Phys. A 778 (2006) 95-123.

[8] D.V. Bugg et al., Nucl. Phys. B 26 (1971) 588-96.

[9] J. Duclos et al., Phys. Lett. B 43 (1973) 245-8.

[10] M. Salomon, D.F. Measday, J-M. Poutissou, B.C. Robertson, Nucl. Phys. A 414 (1984) 493-507.

[11] D.H. Fitzgerald et al., Phys. Rev. C 34 (1986) 619-26.

[12] A. Bagheri et al., Phys. Rev. C 38 (1988) 885-94.

[13] J.C. Staško, Ph.D. dissertation, University of New Mexico, 1993.

[14] E. Frlež et al., Phys. Rev. C 57 (1998) 3144-52.

[15] C.V. Gaulard et al., Phys. Rev. C 60 (1999) 024604.

[16] L.D. Isenhower et al., πN Newsletter 15 (1999) 292-5.

[17] H.-Ch. Schröder et al., Eur. Phys. J. C 21 (2001) 473-88.

[18] M.E. Sadler et al., Phys. Rev. C 69 (2004) 055206.

[19] J. Breitschopf et al., Phys. Lett. B 639 (2006) 424-8.

[20] Y. Jia et al., Phys. Rev. Lett. 101 (2008) 102301.

[21] D. Mekterović et al., Phys. Rev. C 80 (2009) 055207.

[22] G.C. Oades, G. Rasche, W.S. Woolcock, E. Matsinos, A. Gashi, Nucl. Phys. A 794 (2007) 73-86.

[23] R.A. Arndt, W.J. Briscoe, I.I. Strakovsky, R.L. Workman, Phys. Rev. C 74 (2006) 045205; SAID PSA Tool, available at http://gwdac.phys.gwu.edu.

[24] M. Hoferichter, B. Kubis, Ulf-G. Meißner, Phys. Lett. B 678 (2009) 65-71.

[25] S.A. Coon, R.C. Barrett, Phys. Rev. C 36 (1987) 2189-94; T. Goldman, J.A. Henderson, A.W. Thomas, Few-Body Syst. 12 (1992) 123-32; G.A. Miller, Chin. J. Phys. 32 (1994) 1075-87; G.A. Miller, πN Newsletter 11 (1995) 90-5.

[26] R.E. Cutkosky, Phys. Lett. B 88 (1979) 339-42.

[27] T. Meissner, E.M. Henley, Phys. Rev. C 55 (1997) 3093-9.

[28] A. Gashi, E. Matsinos, G.C. Oades, G. Rasche, W.S. Woolcock, Nucl. Phys. A 686 (2001) 447-62; A. Gashi, E. Matsinos, G.C. Oades, G. Rasche, W.S. Woolcock, *ibid.* pp. 463-77.

Table 1

The low-energy CX experiments in chronological order. The first column contains a label identifying the experiment. Columns 2−5 contain the number of measurements reported in each experiment: DCS stands for the differential cross section, LEC for the first three coefficients in the Legendre expansion of the DCS, TCS for the total cross section, and AP for the analysing power. The adjacent column contains the energy or energy range of the experiment; the centre-of-mass scattering angle or angular interval of the measurements is listed in the last column. The experiment of Ref. [17] extracted the scattering length a^{c0} ($= \sqrt{2}b_1$) from a measurement of the width of the $1s$ state in pionic hydrogen; thus, it cannot be placed in any of the categories under Columns $2-5$.

Experiment	DCS	LEC	TCS	AP	T (MeV)	θ
BUGG71 [8]			1		90.90	
DUCLOS73 [9]	3				22.60 − 42.60	180°
SALOMON84 [10]		6			27.40, 39.30	
FITZGERALD86 [11]	21				32.48 − 63.21	9.60 − 25.04°
BAGHERI88 [12]		12			45.60 − 91.70	
STAŠKO93 [13]				4	100.00	75.00 − 130.00°
FRLEŽ98 [14]	6				27.50	4.70 − 50.90°
GAULARD99 [15]				6	98.10	8.02 − 86.05°
ISENHOWER99 [16]	40				10.60 − 39.40	9.60 − 168.24°
SCHROEDER01 [17]					0.00	
SADLER04 [18]	60				63.86 − 94.57	18.19 − 161.81°
BREITSCHOPF06 [19]			9		38.90 − 96.50	
JIA08 [20]	24				34.37 − 59.68	5.81 − 41.39°
MEKTEROVIĆ09 [21]	140				33.89 − 86.62	18.19 − 161.81°

Table 2

The data sets comprising the truncated database for the CX reaction, the pion laboratory kinetic energy T (in MeV), the number of degrees of freedom $(NDF)_j$ for each data set, the scale factor z_j which minimises χ^2_j (Eq. (1) of Ref. [1]), the values of $(\chi^2_j)_{min}$, and the p-value of the fit for each data set. The numbers of this table correspond to the final fit to the data using the K-matrix expansions (see Section 4.1).

Data set	T	$(NDF)_j$	z_j	$(\chi^2_j)_{min}$	p-value	Comments
BUGG71	90.90	1	1.0225	0.1470	0.7014	
DUCLOS73	22.60	1	0.9413	1.2465	0.2642	
DUCLOS73	32.90	1	0.9717	0.2700	0.6033	
DUCLOS73	42.60	1	0.9098	2.3836	0.1226	
SALOMON84	27.40	3	0.9720	2.8685	0.4124	
SALOMON84	39.30	3	0.9937	1.0774	0.7825	
FITZGERALD86	32.48	2	1.5076	2.3635	0.3067	freely floated
FITZGERALD86	36.11	2	1.7103	1.1845	0.5531	freely floated
FITZGERALD86	40.26	2	1.8274	6.1362	0.0465	freely floated
FITZGERALD86	47.93	2	1.4497	1.5402	0.4630	freely floated
FITZGERALD86	51.78	3	1.1236	7.3728	0.0609	
FITZGERALD86	55.58	3	1.0926	2.5611	0.4644	
FITZGERALD86	63.21	3	1.0503	1.2246	0.7471	
BAGHERI88	45.60	3	1.0056	0.1314	0.9878	
BAGHERI88	62.20	3	0.9589	3.4999	0.3208	
BAGHERI88	76.40	3	0.9731	3.2706	0.3518	
BAGHERI88	91.70	3	1.0151	2.8032	0.4230	
STAŠKO93	100.00	4	0.9948	1.4336	0.8383	
FRLEŽ98	27.50	6	1.0902	10.2313	0.1152	
GAULARD99	98.10	6	1.0241	1.1007	0.9815	
ISENHOWER99	10.60	4	1.0203	2.1816	0.7024	
ISENHOWER99	10.60	5	1.0054	1.4611	0.9175	
ISENHOWER99	10.60	6	1.0181	8.0844	0.2320	
ISENHOWER99	20.60	5	0.9803	1.5435	0.9080	
ISENHOWER99	20.60	6	1.0120	8.1813	0.2251	

Table 1 continued

Data set	T	$(NDF)_j$	z_j	$(\chi^2_j)_{min}$	p-value	Comments
ISENHOWER99	39.40	4	1.0701	7.1132	0.1300	
ISENHOWER99	39.40	5	1.0597	8.4184	0.1346	
ISENHOWER99	39.40	5	0.9514	5.1617	0.3965	
SCHROEDER01	0.00	1	0.9747	2.5184	0.1125	
SADLER04	63.86	20	0.9548	16.0803	0.7116	
SADLER04	83.49	20	0.9881	11.6506	0.9276	
SADLER04	94.57	20	1.0296	7.2573	0.9958	
BREITSCHOPF06	38.90	1	0.9960	0.1643	0.6852	
BREITSCHOPF06	43.00	1	1.0011	0.0259	0.8721	
BREITSCHOPF06	47.10	1	0.9981	0.0572	0.8110	
BREITSCHOPF06	55.60	1	0.9952	0.2074	0.6488	
BREITSCHOPF06	64.30	1	0.9725	3.7739	0.0521	
BREITSCHOPF06	65.90	1	0.9779	2.3441	0.1258	
BREITSCHOPF06	76.10	1	0.9814	1.6114	0.2043	
BREITSCHOPF06	96.50	1	0.9816	0.6152	0.4328	
JIA08	34.37	4	0.8434	4.9306	0.2945	
JIA08	39.95	4	0.8680	3.1715	0.5295	
JIA08	43.39	4	0.8777	2.5167	0.6416	
JIA08	46.99	4	0.9798	5.1175	0.2754	
JIA08	54.19	4	0.9080	2.0430	0.7279	
JIA08	59.68	4	0.9265	3.2449	0.5177	
MEKTEROVIĆ09	33.89	20	1.0239	17.0075	0.6525	
MEKTEROVIĆ09	39.38	20	1.0145	14.7514	0.7905	
MEKTEROVIĆ09	44.49	20	1.0100	33.1457	0.0325	
MEKTEROVIĆ09	51.16	20	1.0357	15.0473	0.7737	
MEKTEROVIĆ09	57.41	20	1.0394	19.9034	0.4640	
MEKTEROVIĆ09	66.79	20	1.0235	19.4707	0.4914	
MEKTEROVIĆ09	86.62	20	1.0019	31.1877	0.0528	

Table 3

The values of the seven parameters of the ETH model obtained from the common fit to the truncated $\pi^+ p$ and CX databases (ZUAS12a solution). The ZUAS12 solution [1], obtained from the fits to the $\pi^{\pm} p$ elastic-scattering data for $p_{min} \approx 1.24 \cdot 10^{-2}$, is shown for comparison.

	This work (ZUAS12a)	ZUAS12
$G_\sigma(GeV^{-2})$	29.6 ± 1.9	27.48 ± 0.86
K_σ	0.117 ± 0.054	0.016 ± 0.034
$G_\rho(GeV^{-2})$	59.36 ± 0.57	54.67 ± 0.61
K_ρ	1.34 ± 0.29	0.66 ± 0.41
$g_{\pi NN}$	13.43 ± 0.11	12.84 ± 0.12
$g_{\pi N\Delta}$	29.07 ± 0.28	29.77 ± 0.26
Z	-0.393 ± 0.086	-0.552 ± 0.056

Table 4

The correlation matrix for the seven parameters of the ETH model for the common fit to the truncated $\pi^+ p$ and CX databases.

	G_σ	K_σ	G_ρ	K_ρ	$g_{\pi NN}$	$g_{\pi N\Delta}$	Z
G_σ	1.0000	0.5620	0.1167	0.2311	0.3777	−0.4932	−0.2225
K_σ	0.5620	1.0000	0.7092	0.8642	0.8280	−0.9501	0.6588
G_ρ	0.1167	0.7092	1.0000	0.7219	0.8386	−0.7537	0.7780
K_ρ	0.2311	0.8642	0.7219	1.0000	0.7628	−0.8591	0.8060
$g_{\pi NN}$	0.3777	0.8280	0.8386	0.7628	1.0000	−0.9024	0.6317
$g_{\pi N\Delta}$	−0.4932	−0.9501	−0.7537	−0.8591	−0.9024	1.0000	−0.6497
Z	−0.2225	0.6588	0.7780	0.8060	0.6317	−0.6497	1.0000

Table 5

The various χ^2 values obtained in the analysis of the low-energy πN data, along with the number of degrees of freedom in each fit, for three values of p_{min} (the confidence level in the statistical tests); these three p_{min} values correspond to a 3, 2.5, and 2σ effect in the normal distribution, respectively. The definitions of the databases (DB) are given at the end of Section 2. Separate fits to the three databases using the ETH model are not attempted, given the largeness of the correlations among the model parameters in that case.

Parametric model	DB_+ [1]	DB_- [1]	DB_0 (this work)	$DB_{+/-}$ [1]	$DB_{+/0}$ (this work)
$p_{min} \approx 2.70 \cdot 10^{-3}$ (3σ)					
K-matrix	434.4/334	397.9/325	333.4/323	825.9/659	765.1/657
ETH model	–	–	–	905.4/666	969.8/664
$p_{min} \approx 1.24 \cdot 10^{-2}$ (2.5σ)					
K-matrix	427.2/333	371.0/321	312.8/321	792.4/654	737.0/654
ETH model	–	–	–	872.9/661	932.3/661
$p_{min} \approx 4.55 \cdot 10^{-2}$ (2σ)					
K-matrix	357.0/310	332.3/316	306.4/320	684.4/626	663.3/630
ETH model	–	–	–	755.2/633	814.6/637

Table 6

The values of the six s- and p-wave em-modified hadronic phase shifts (in degrees), obtained on the basis of the results of Tables 3 (ZUAS12a solution) and 4.

$T(MeV)$	$\tilde{\delta}_{0+}^{3/2}$ (S31)	$\tilde{\delta}_{0+}^{1/2}$ (S11)	$\tilde{\delta}_{1+}^{3/2}$ (P33)	$\tilde{\delta}_{1-}^{3/2}$ (P31)	$\tilde{\delta}_{1+}^{1/2}$ (P13)	$\tilde{\delta}_{1-}^{1/2}$ (P11)
20	−2.456(49)	4.565(61)	1.3239(89)	−0.2390(71)	−0.1694(62)	−0.430(13)
25	−2.861(51)	5.092(65)	1.877(12)	−0.329(10)	−0.2293(87)	−0.569(18)
30	−3.260(52)	5.562(68)	2.507(15)	−0.425(13)	−0.292(11)	−0.708(24)
35	−3.658(53)	5.988(71)	3.212(17)	−0.528(17)	−0.357(15)	−0.843(30)
40	−4.055(53)	6.376(73)	3.996(20)	−0.635(21)	−0.423(18)	−0.973(37)
45	−4.455(54)	6.733(76)	4.861(22)	−0.747(25)	−0.489(22)	−1.095(44)
50	−4.858(56)	7.062(81)	5.810(24)	−0.863(30)	−0.556(25)	−1.208(52)
55	−5.264(58)	7.366(86)	6.849(25)	−0.982(35)	−0.622(29)	−1.310(60)
60	−5.673(62)	7.647(92)	7.985(27)	−1.104(40)	−0.688(34)	−1.401(69)
65	−6.087(68)	7.907(99)	9.222(30)	−1.229(46)	−0.753(38)	−1.479(78)
70	−6.504(75)	8.15(11)	10.571(33)	−1.356(52)	−0.817(43)	−1.543(87)
75	−6.925(84)	8.37(12)	12.038(38)	−1.486(58)	−0.880(48)	−1.593(98)
80	−7.350(94)	8.57(13)	13.635(45)	−1.617(64)	−0.942(54)	−1.63(11)
85	−7.78(11)	8.76(14)	15.372(55)	−1.751(71)	−1.003(59)	−1.65(12)
90	−8.21(12)	8.93(16)	17.261(68)	−1.885(79)	−1.061(65)	−1.65(13)
95	−8.65(13)	9.09(17)	19.315(84)	−2.022(86)	−1.118(71)	−1.64(14)
100	−9.08(15)	9.23(19)	21.55(10)	−2.159(94)	−1.174(77)	−1.61(16)

Table 7

The scale factors $\hat{z}_j$ for free floating for the CX data sets, obtained on the basis of the ZUAS12 solution [1], listed separately for the differential cross sections (upper part), total cross sections (second part), analysing powers (third part), and the results for the coefficients of the Legendre expansion of the differential cross section (last part). The four FITZGERALD86 data sets which had been floated freely in Section 4.1 have not been included. Not listed in the table is also the result of Ref. [17] for the isovector scattering length b_1. The quantity $\Delta\hat{z}_j$ is the total uncertainty (see end of Section 2.2 of Ref. [1]).

Data set	T (MeV)	$\hat{z}_j$	$\Delta\hat{z}_j$
DUCLOS73	22.60	1.03	0.14
DUCLOS73	32.90	1.09	0.13
DUCLOS73	42.60	0.95	0.12
FITZGERALD86	51.78	1.29	0.10
FITZGERALD86	55.58	1.252	0.099
FITZGERALD86	63.21	1.204	0.093
FRLEŽ98	27.50	1.431	0.099
ISENHOWER99	10.60	1.45	0.12
ISENHOWER99	10.60	1.332	0.081
ISENHOWER99	10.60	1.307	0.057
ISENHOWER99	20.60	1.205	0.052
ISENHOWER99	20.60	1.229	0.047
ISENHOWER99	39.40	1.47	0.11
ISENHOWER99	39.40	1.245	0.045
ISENHOWER99	39.40	1.089	0.042
SADLER04	63.86	1.050	0.068
SADLER04	83.49	1.045	0.053
SADLER04	94.57	1.063	0.047
JIA08	34.37	1.04	0.11
JIA08	39.95	1.00	0.12
JIA08	43.39	0.94	0.13
JIA08	46.99	1.09	0.14
JIA08	54.19	0.94	0.13
JIA08	59.68	0.99	0.12

Table 6 continued

Data set	T (MeV)	$\hat{z}_j$	$\Delta\hat{z}_j$
MEKTEROVIĆ09	33.89	1.213	0.040
MEKTEROVIĆ09	39.38	1.182	0.032
MEKTEROVIĆ09	44.49	1.160	0.031
MEKTEROVIĆ09	51.16	1.181	0.033
MEKTEROVIĆ09	57.41	1.168	0.031
MEKTEROVIĆ09	66.79	1.127	0.032
MEKTEROVIĆ09	86.62	1.056	0.030
BUGG71	90.90	1.068	0.061
BREITSCHOPF06	38.90	1.12	0.10
BREITSCHOPF06	43.00	1.17	0.15
BREITSCHOPF06	47.10	1.11	0.12
BREITSCHOPF06	55.60	1.078	0.094
BREITSCHOPF06	64.30	0.967	0.069
BREITSCHOPF06	65.90	0.995	0.067
BREITSCHOPF06	76.10	0.994	0.065
BREITSCHOPF06	96.50	0.999	0.039
STAŠKO93	100.00	0.91	0.11
GAULARD99	98.10	0.961	0.058
SALOMON84	27.40	1.099	0.056
SALOMON84	39.30	1.132	0.059
BAGHERI88	45.60	1.149	0.036
BAGHERI88	62.20	1.042	0.039
BAGHERI88	76.40	1.038	0.036
BAGHERI88	91.70	1.063	0.039

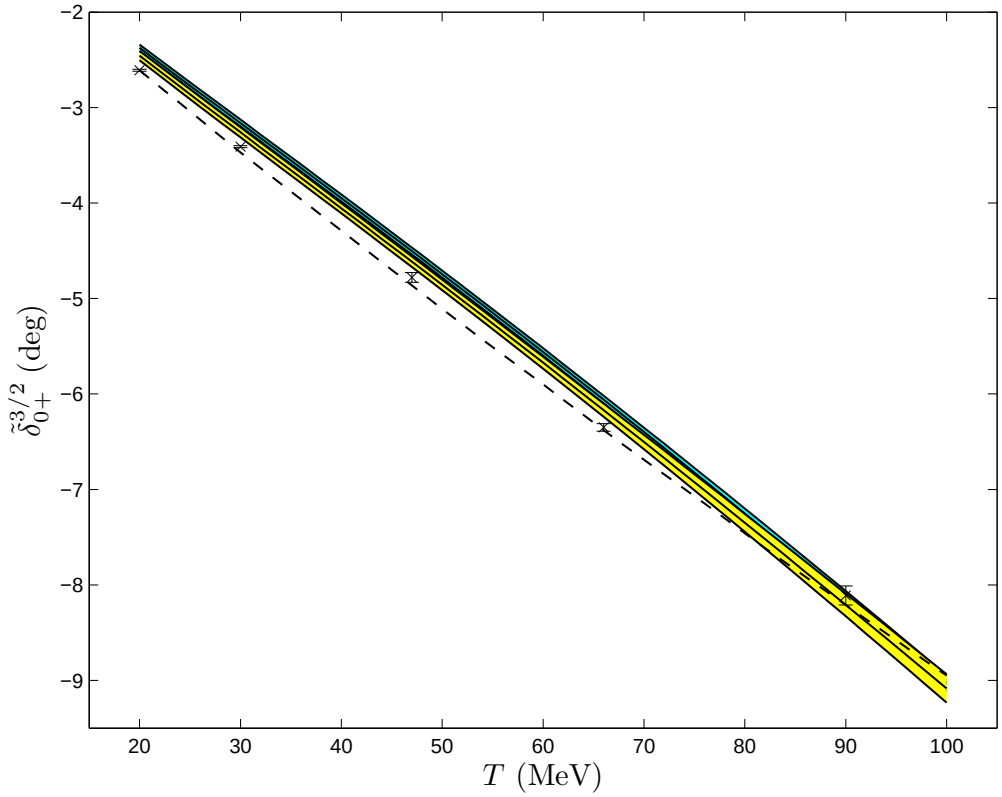

Fig. 1. The em-modified hadronic phase shift $\tilde{\delta}_{0+}^{3/2}$ (S31) from the present work, along with 1σ uncertainties (yellow band). Shown is also the ZUAS12 solution [1], obtained on the basis of the elastic-scattering data below 100 MeV, along with the corresponding 1σ uncertainties (blue band). The current SAID solution (WI08) [23] is represented by the dashed curve; their five single-energy values (at $T = 20$, 30, 47, 66, and 90 MeV) are also shown.

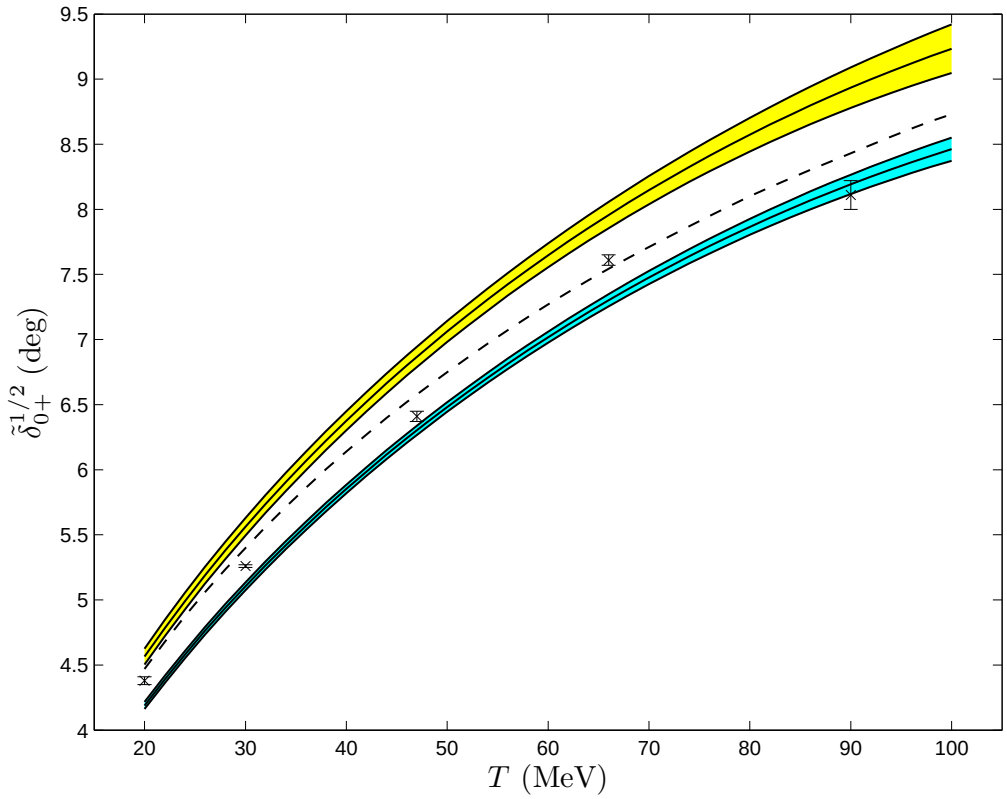

Fig. 2. The em-modified hadronic phase shift $\tilde{\delta}_{0+}^{1/2}$ (S11) from the present work, along with 1σ uncertainties (yellow band). Shown is also the ZUAS12 solution [1], obtained on the basis of the elastic-scattering data below 100 MeV, along with the corresponding 1σ uncertainties (blue band). The current SAID solution (WI08) [23] is represented by the dashed curve; their five single-energy values (at $T = 20$, 30, 47, 66, and 90 MeV) are also shown.

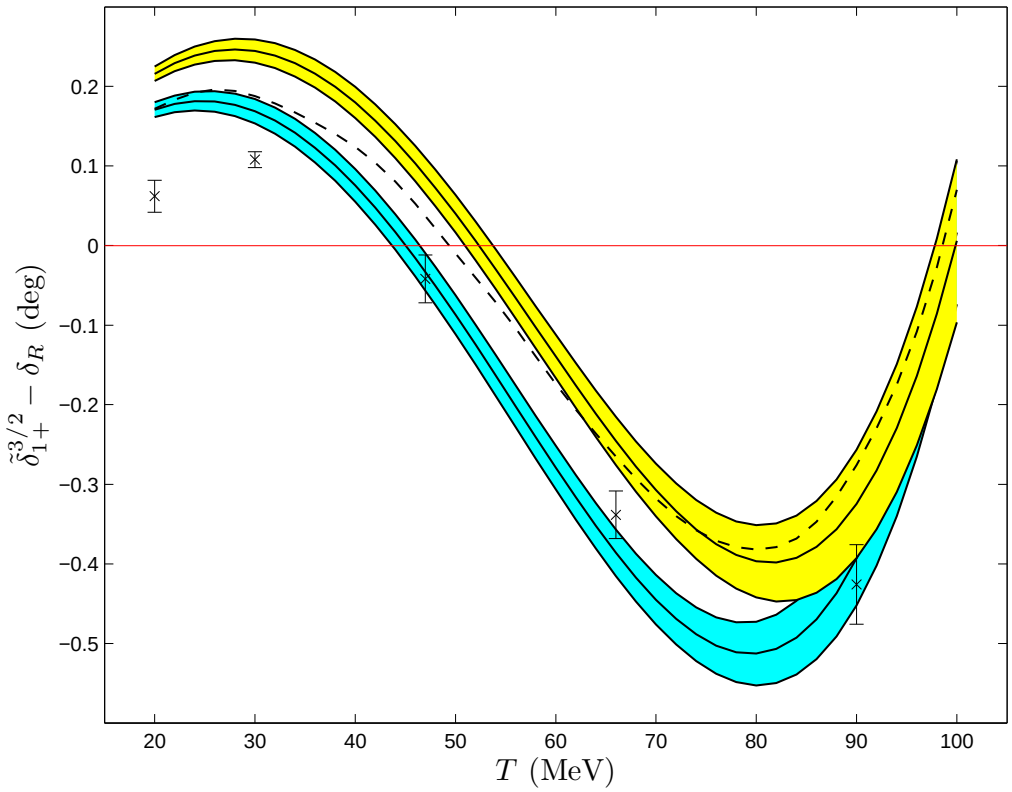

Fig. 3. The em-modified hadronic phase shift $\tilde{\delta}_{1+}^{3/2}$ (P33) from the present work, along with 1σ uncertainties (yellow band). Shown is also the ZUAS12 solution [1], obtained on the basis of the elastic-scattering data below 100 MeV, along with the corresponding 1σ uncertainties (blue band). The current SAID solution (WI08) [23] is represented by the dashed curve; their five single-energy values (at $T = 20$, 30, 47, 66, and 90 MeV) are also shown. To enable the meaningful comparison of the values contained in this figure, an energy-dependent baseline δ_R ($= (0.20 \cdot T + 1.54) T \cdot 10^{-2}$, with T in MeV and $\delta_R(T)$ in degrees) was subtracted from all data.

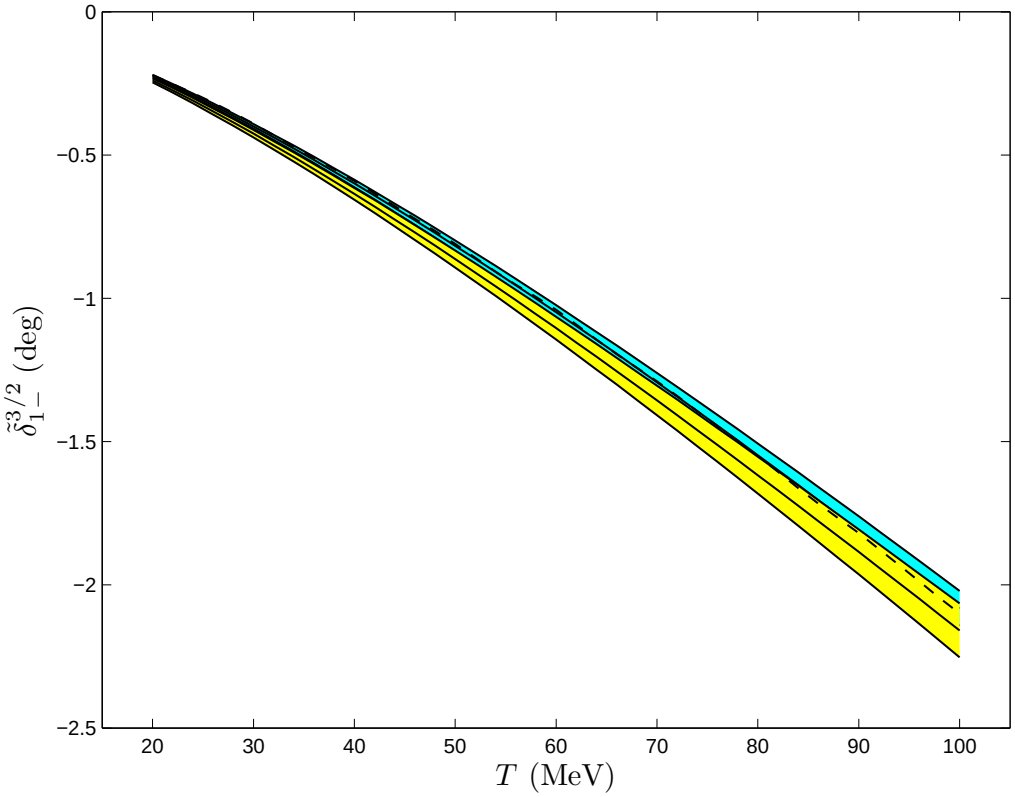

Fig. 4. The em-modified hadronic phase shift $\tilde{\delta}_{1-}^{3/2}$ (P31) from the present work, along with 1σ uncertainties (yellow band). Shown is also the ZUAS12 solution [1], obtained on the basis of the elastic-scattering data below 100 MeV, along with the corresponding 1σ uncertainties (blue band). The current SAID solution (WI08) [23] is represented by the dashed curve.

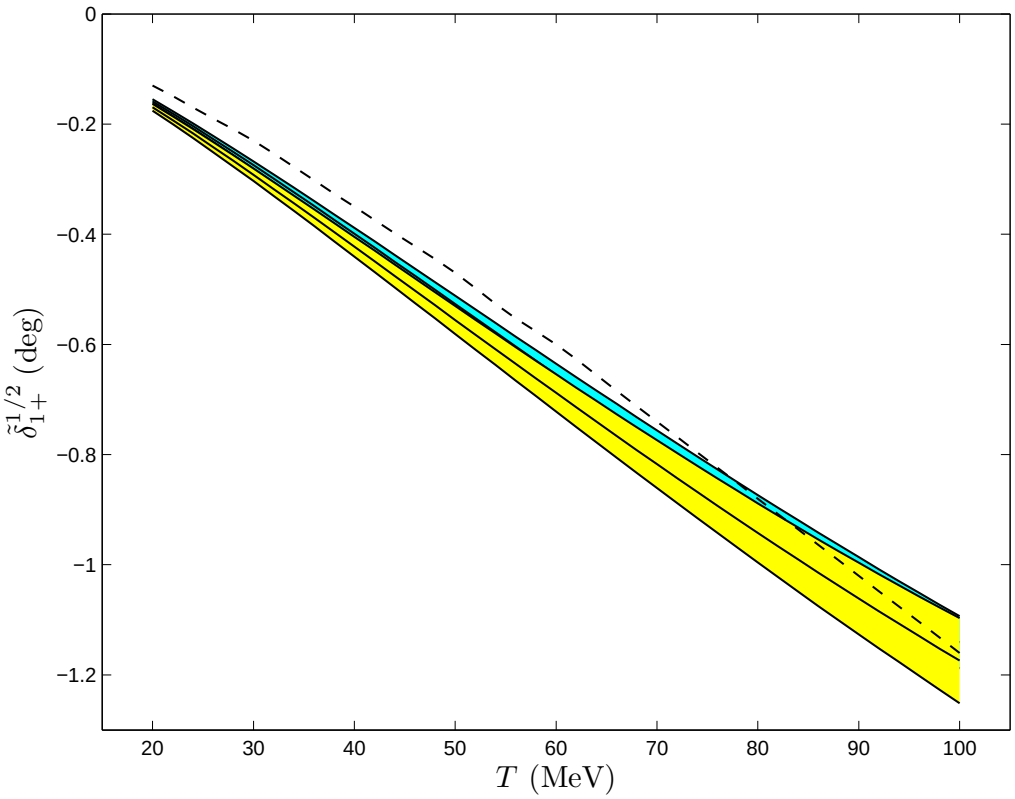

Fig. 5. The em-modified hadronic phase shift $\tilde{\delta}_{1+}^{1/2}$ (P13) from the present work, along with 1σ uncertainties (yellow band). Shown is also the ZUAS12 solution [1], obtained on the basis of the elastic-scattering data below 100 MeV, along with the corresponding 1σ uncertainties (blue band). The current SAID solution (WI08) [23] is represented by the dashed curve.

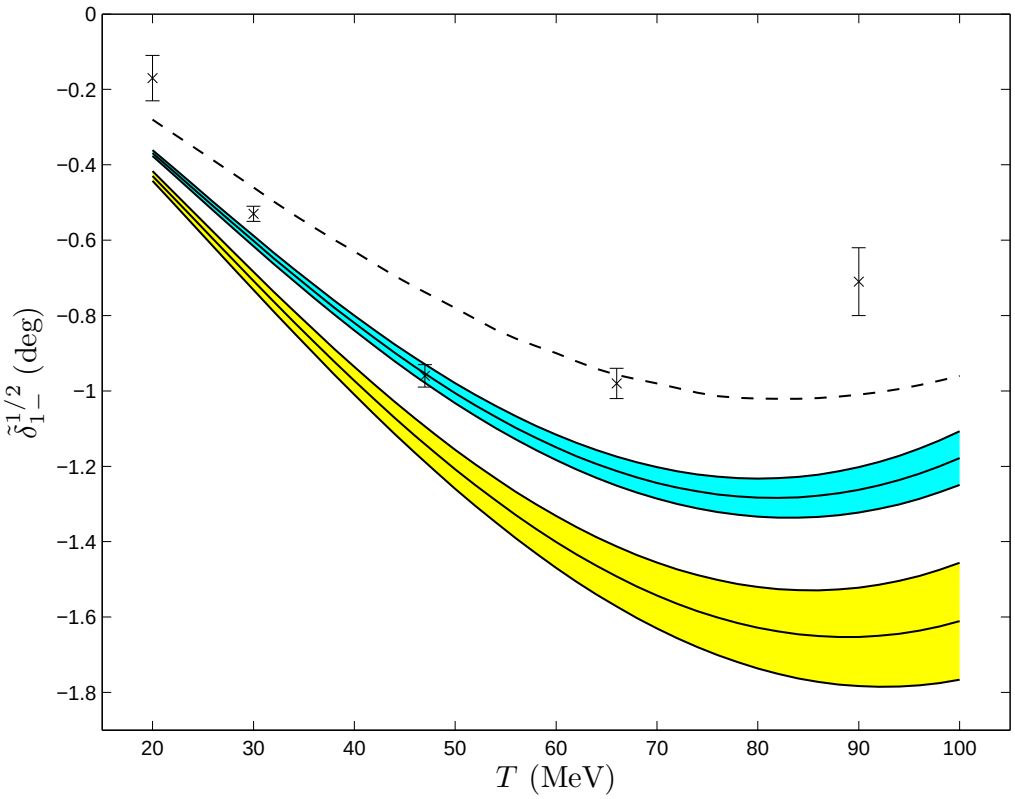

Fig. 6. The em-modified hadronic phase shift $\tilde{\delta}_{1-}^{1/2}$ (P11) from the present work, along with 1σ uncertainties (yellow band). Shown is also the ZUAS12 solution [1], obtained on the basis of the elastic-scattering data below 100 MeV, along with the corresponding 1σ uncertainties (blue band). The current SAID solution (WI08) [23] is represented by the dashed curve; their five single-energy values (at $T = 20$, 30, 47, 66, and 90 MeV) are also shown.

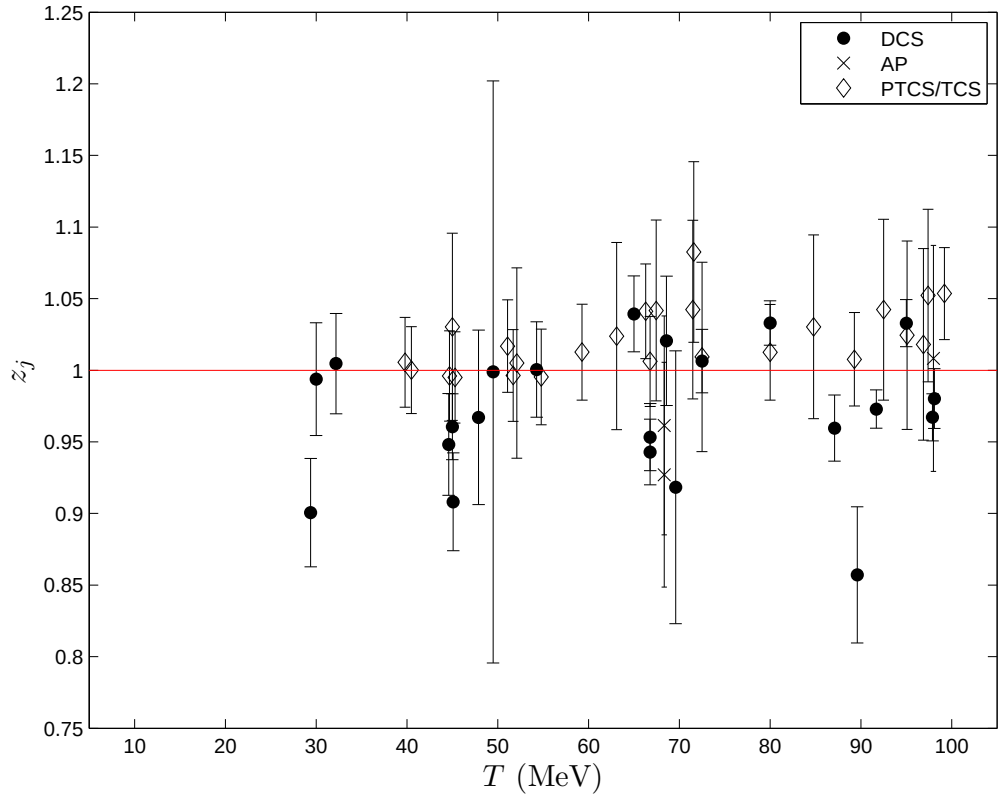

Fig. 7. The scale factors z_j for the π^+p data, obtained from the common fit to the truncated π^+p and CX databases using the ETH model (see Section 4.2). The values, corresponding to the two data sets which were freely floated (see Table 1 of Ref. [1]), have not been included.

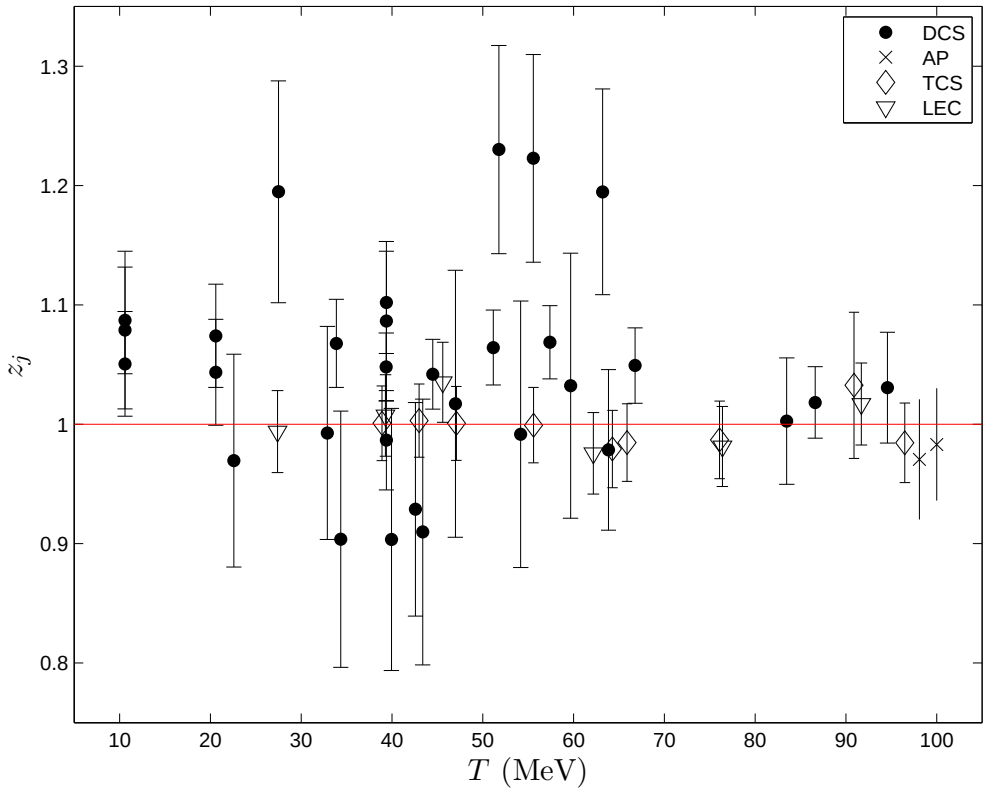

Fig. 8. The scale factors z_j for the CX data, obtained from the common fit to the truncated π^+p and CX databases using the ETH model (see Section 4.2). The values, corresponding to the four data sets which were freely floated (see Table 2), have not been included. The data sets with the largest scale factors z_j are the three FITZGERALD86 data sets which were not freely floated, as well as the FRLEŽ98 data set.

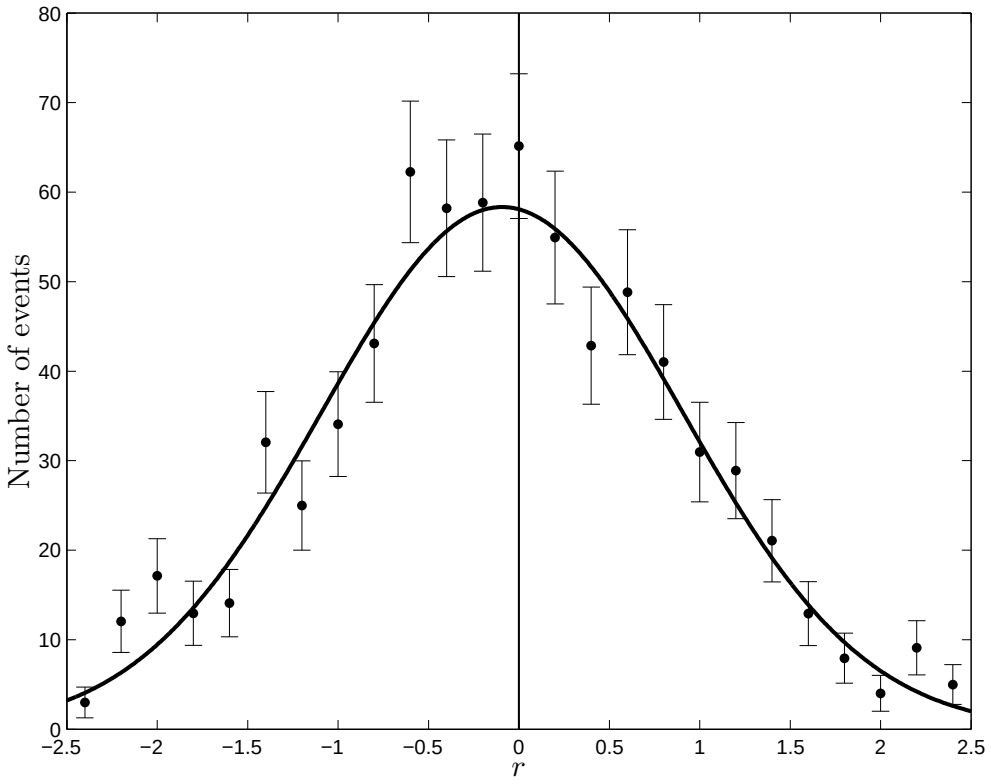

Fig. 9. The distribution of the normalised residuals, obtained from the common fit to the truncated $\pi^+ p$ and CX databases using the ETH model (see Section 4.2). Also shown (solid curve) is the optimal Gaussian fit to the data.

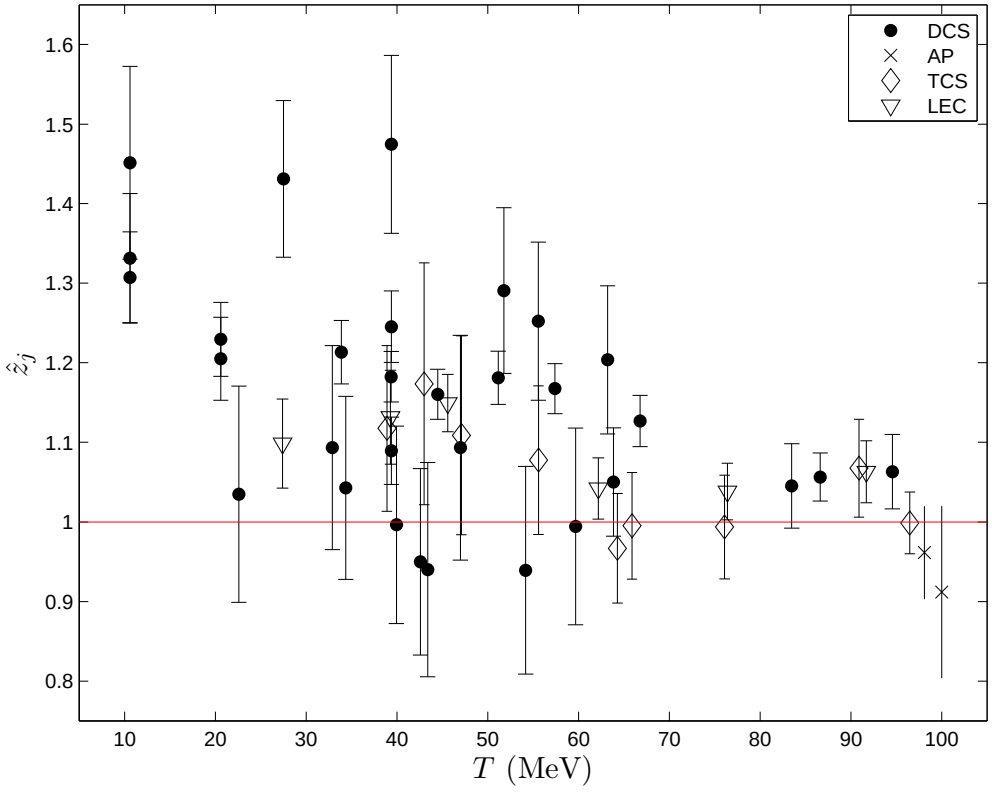

Fig. 10. The scale factors $\hat{z}_j$ for free floating (evaluated with Eq.(5) of Ref. [1]) for the CX data sets, obtained on the basis of the ZUAS12 solution [1], plotted separately for differential cross sections (DCS), total cross sections (TCS), analysing powers (AP), and the results for the coefficients of the Legendre expansion of the DCS (LEC). The four FITZGERALD86 data sets, which had been freely floated (see Table 2), are not shown. Not shown in the figure is also the result of Ref. [17] for the isovector scattering length b_1.

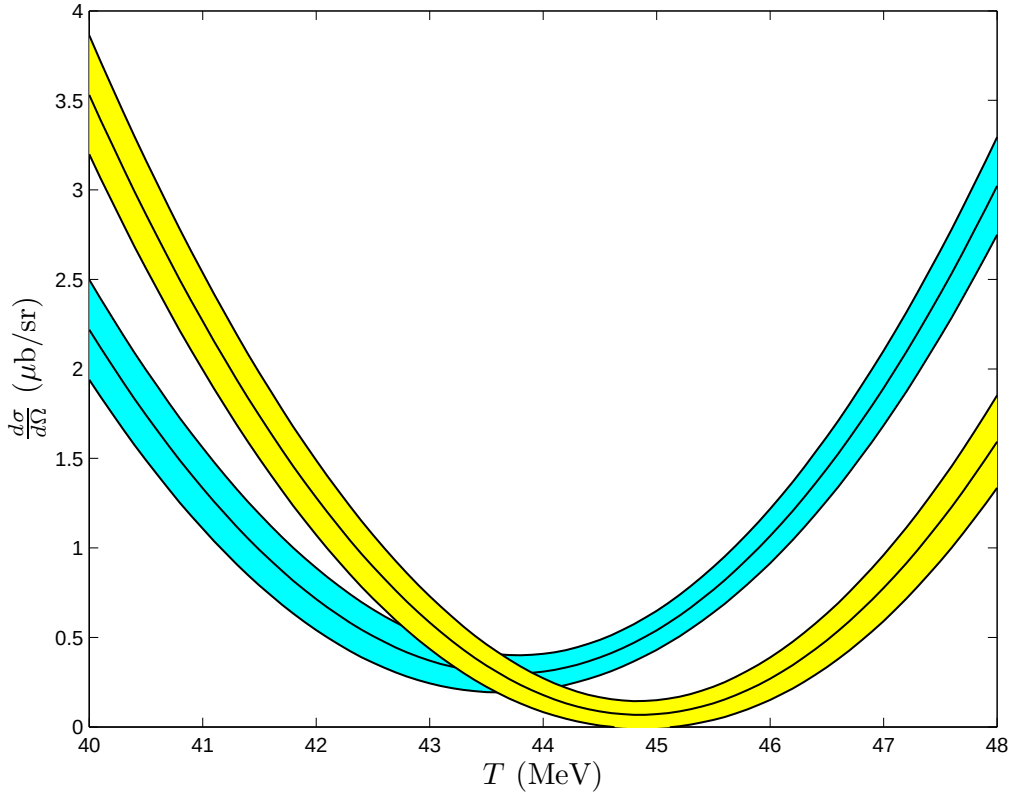

Fig. 11. Our two predictions corresponding to the CX DCS for centre-of-mass scattering angle $\theta = 0^\circ$ around the s- and p-wave interference minimum. The ZUAS12 prediction [1] is represented by the blue band, whereas the ZUAS12a one (this work) by the yellow band. Both bands indicate 1σ uncertainties.

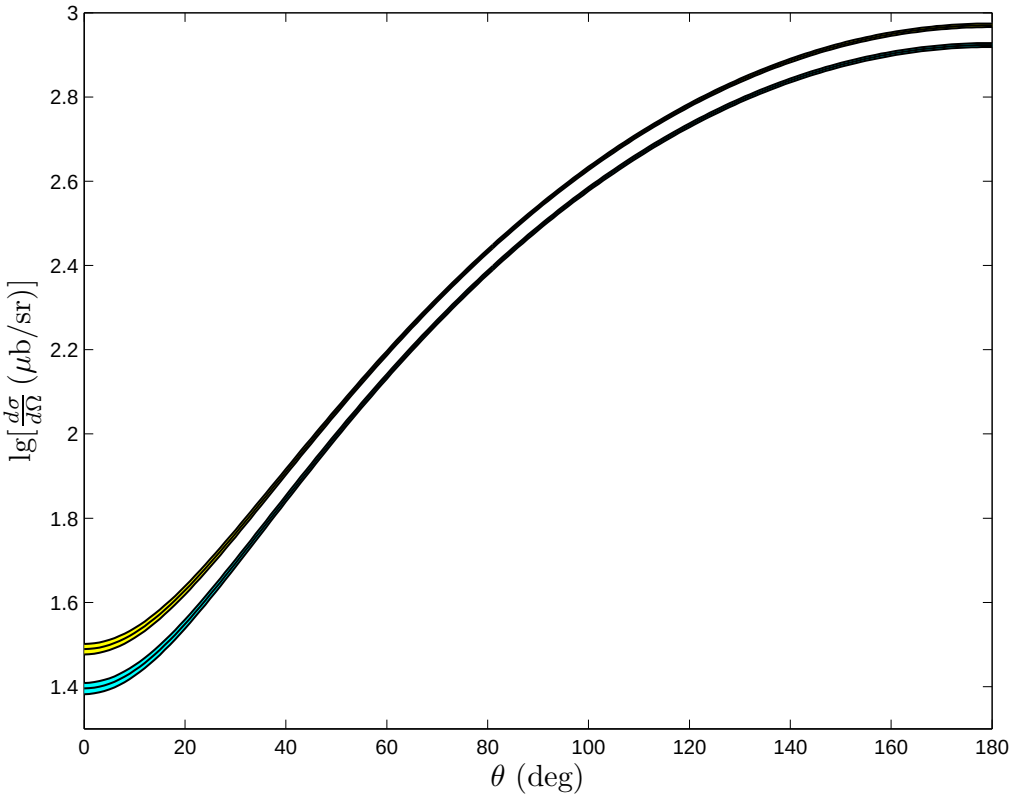

Fig. 12. Our two predictions corresponding to the CX DCS at 30 MeV; θ denotes the centre-of-mass scattering angle. The ZUAS12 prediction [1] is represented by the blue band, whereas the ZUAS12a one (this work) by the yellow band. Both bands indicate 1σ uncertainties.

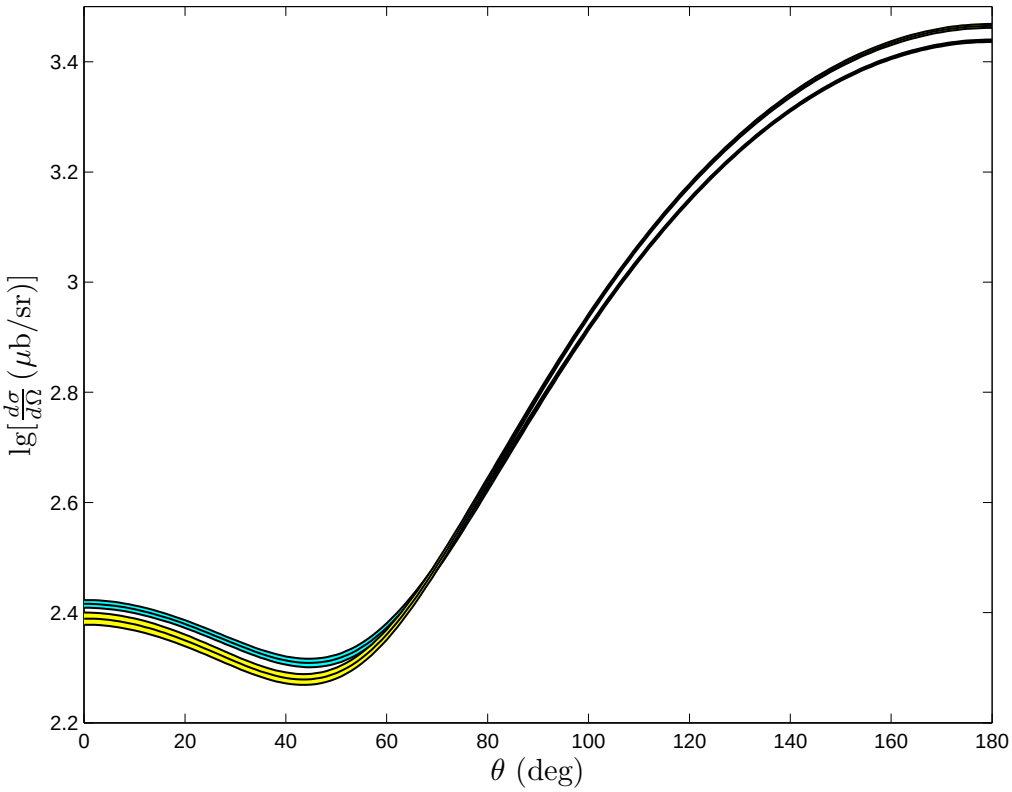

Fig. 13. Our two predictions corresponding to the CX DCS at 80 MeV; θ denotes the centre-of-mass scattering angle. The ZUAS12 prediction [1] is represented by the blue band, whereas the ZUAS12a one (this work) by the yellow band. Both bands indicate 1σ uncertainties.

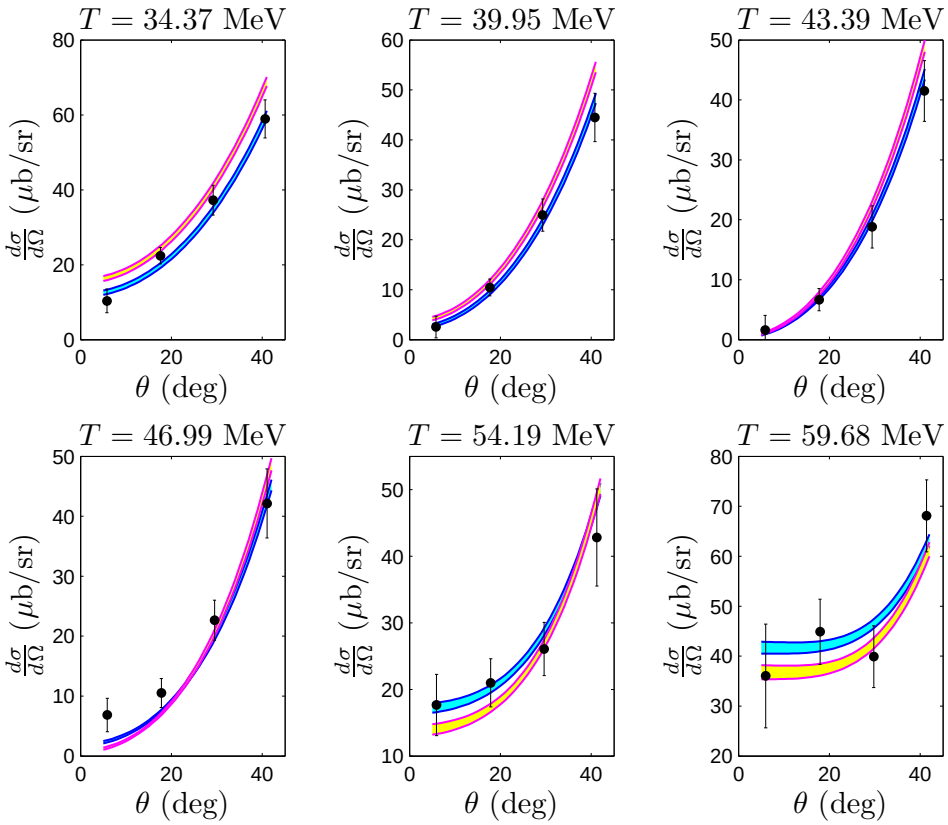

Fig. 14. Our two predictions corresponding to the CX DCS in the kinematical region of the JIA08 [20] experiment. The ZUAS12 prediction [1] is represented by the blue band, whereas the ZUAS12a one (this work) by the yellow band. Both bands indicate 1σ uncertainties. Not included in the uncertainty of their data is the 10% normalisation uncertainty of the experiment of Ref. [20].

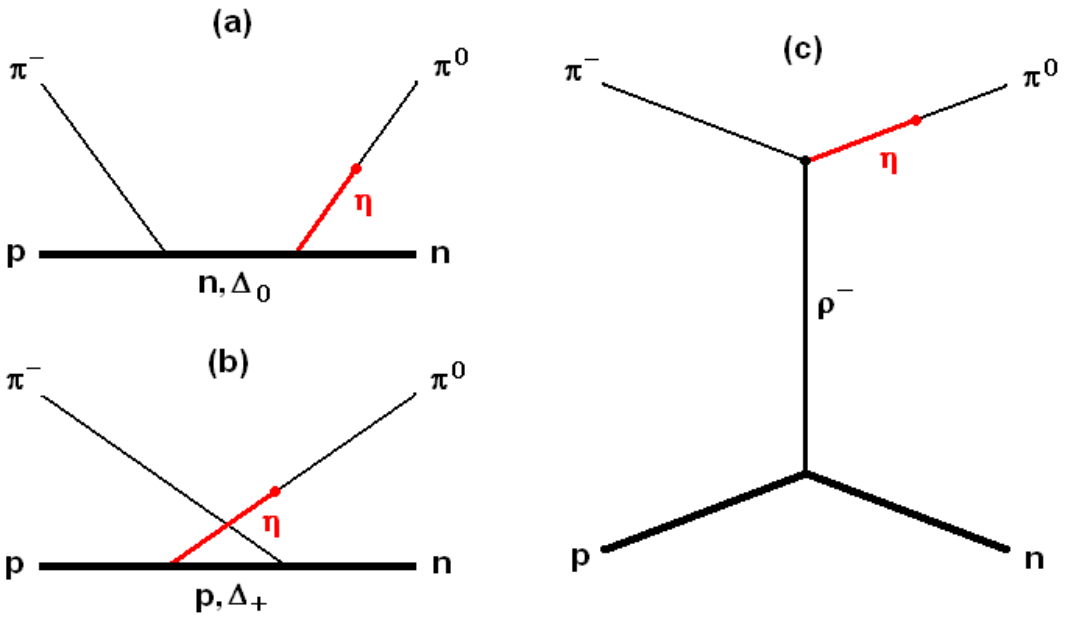

Fig. 15. Influence of the $\eta - \pi^0$ mixing on the Feynman diagrams of the ETH model in case of the CX reaction.